BABAR Analysis Document 1086, Version 6
January 27, 2005

Extraction of the CKM angle γ in $B^- \to D^{(*)}K^-$ decays using a D^0 Dalitz plot analysis technique (Document 2)

M.Carpinelli[2],G.Cavoto[3,4],M.Giorgi[2],
X.Giroux[1],Y.P. Lau[3],L.Li Gioi[4],F.Martinez-Vidal[2,5],
N.Neri[2],J.Olsen[3],E.Prencipe[4],M.Rama[2],M.H.Schune[1],
A.Stocchi[1]

[1] *Laboratoire de l'Accélérateur Linéaire, Orsay, France*
[2] *Università di Pisa & INFN Pisa, Italy*
[3] *Princeton University, Princeton, NJ, USA*
[4] *Università di Roma "La Sapienza" & INFN Roma I, Italy*
[5] *& IFIC/CSIC Valencia, Spain*

Abstract

This note describes the second part of the analysis used to extract the CKM angle γ from the study of $B^- \to D^{(*)0}K^-$ (with $D^* \to D^0\pi^0, D^0\gamma$) decays using a Dalitz plot analysis technique of $D^0 \to K_S\pi^+\pi^-$ decays. This document focus on the description of the final *CP* fit configuration, results and systematic uncertainties, along with the statistical methods (frequentist and Bayesian) used to extract the final value of γ and the other *CP*-violating parameters. The first supporting document (BAD#899) describes the analysis setup, event selection and background characterization, likelihood fit procedure, Dalitz model and some fit results. We adopt the frequentist approach to provide final results, while the Bayesian method is used as an independent cross-check. The final results of the analysis are also presented and discussed here. We use Run1-2-3-4(BlackDiamond) data corresponding to an integrated luminosity of 205 fb^{-1}.

Contents

List of Figures

List of Tables

1 Introduction

The likelihood function used for the measurement of the angle γ of the CKM unitarity triangle making use of D^0 three-body decays (such as $D^0 \to K^0_S\pi^+\pi^-$) from $B^- \to D^{(*)}K^-$ decays through a Dalitz analysis [1] is affected by large non-Gaussian effects for the current statistics (205 fb^{-1}) [2]. We observe that for a relatively small dataset and for small absolute value of the ratio of the $A(b \to u)$ and $A(b \to c)$ amplitudes, $r_B = |A(b \to u)/A(b \to c)|$, the likelihood fit returns a biased estimate of r_B, and the rms of γ (the CKM weak phase) and δ (the strong phase of the B decay) pulls are significantly larger than unity. This is easily understood since $\sigma^2(\gamma)$ is proportional to $\frac{1}{\frac{d^2logL}{d^2\gamma}}$, and $\frac{d^2logL}{d^2\gamma}$ is proportional to r_B, therefore it will be smaller for larger r_B. Since there r_B is positively biased the error returned by the maximum likelihood method will be smaller than what it should be to represent the statistical fluctuation (i.e. it does not define a confidence interval with the correct coverage properties). Moreover, while the linearity of γ and δ is verified, r_B saturates at low truth values of r_B, with a saturation region different for the different samples since they have different statistical contents. The saturation effect, the r_B bias and the large γ and δ pulls essentially go away with a data sample about ten times larger. The nature of these non-Gaussian effects scaling with the size of the data sample are related to the small number of events in the region of the Dalitz plot sensitive to r_B (and γ) and to the polar coordinates representation of the space of fit parameters, and more particularly, to the positive definiteness of r_B.

As a consequence, the usual assumption that the parameters at the maximum of the likelihood are unbiased estimators of true quantities it is not valid anymore, and more sophisticated techniques are needed to extract central values, errors and confidence intervals [3]. This also poses limitations to the way how systematic uncertainties have to be evaluated. For example, usual techniques based on the quadratic differences of fit errors between the nominal and alternative fit configurations are now not reliable since fit errors are not a good representation of the true statistical fluctuations. Similarly, one has to be very careful when looking at differences in central values since biases themselves are a function of the truth values. Thus we have employed and developed both frequentist and Bayesian techniques to extract the confidence intervals, central values and errors, which are described in this document. Since the frequestist approach has several advantages for the extraction of both statistical and systematic uncertainties (in addition to avoiding the intrinsic arbitrary choice of the prior distributions of Bayesian methods) we have used it for presenting the final analysis results on r_B, γ and δ, using the Bayesian approach as an independent cross-check. The systematic uncertainties assigned to the Bayesian results are those obtained with the frequentist method, since the correct evaluation of these errors require the use of cartesian coordinates, which imply the use of the frequentist approach.

In the classical (frequentist) approach, the confidence interval $[p_1, p_2]$ for parameter p, whose true value p^t is unknown, is such that has a probability

$$P(p \in [p_1, p_2]) = 1 - \alpha, \tag{1}$$

of containing the unknown true value. The limits of the interval, p_1 and p_2, are functions of the measured value of p. In particular the confidence interval will contain the unknown true point p^t in a fraction $1-\alpha$ of the experiments, or in other words, if the experiment is carried out many times, a fraction $1-\alpha$ of those experiments will find the measured point within the given confidence region. If Eq. (1) is satisfied, one can say that the defined interval *covers* at the stated confidence level, or that the interval has the correct *coverage*. In our case we have not 1-dimensional confidence level interval but a 3-dimensional or 5-dimensional confidence level regions, as the unknown vector parameters of parameters is

$$\mathbf{p}^{\mathrm{t}} = (r_B^t, \gamma^t, \delta^t) \qquad \text{or} \qquad \mathbf{p}^{\mathrm{t}} = (r_B^t, \gamma^t, \delta^t, r_B^{*t}, \delta^{*t}) \ . \tag{2}$$

The 3-dimensional (5-dimensional) confidence level regions determined are $\alpha = 19.9\%$, 72.1% (3.7%, 42.8%) corresponding to 1, 1.96 standard deviations respectively for each single parameter (regardless the others), in the case of a 3-dimensional (5-dimensional) Gaussian distribution[1]. We will quote finally for the error on the single parameters the statistical error corresponding to the 19.9% confidence region (1 standard deviation ellipsoid). The methodology used is similar to that used by Belle [4] although with some relevant differences, and requires knowledge of the probability density function, PDF, of the fitted parameters $\mathbf{z}$, as a function of the true parameters $\mathbf{p}^{\mathrm{t}}$. This PDF can be obtained using toy MC techniques, where large sets of experiments are generated and fitted using the full experimental likelihood function $\mathcal{L}_{exp}$, as will be discussed in section 2.2.

Alternatively, if we interpret the likelihood function as a probability density function for the truth parameters, a correct estimator can be given by the average value of each parameter according to its own PDF. This method to obtain an *a posteriori* distribution for each parameter requires an *a priori* distribution, which will be assumed as flat in the space of polar coordinates. This arbitrary choice is intrinsic to Bayesian methods [3], but it still can provide reliable estimates of the confidence intervals if the dependence with the *a priori* distribution is small. As indicated previously, the Bayesian approach is used as an independent cross-check of the frequentist results.

[1] Or equivalently, χ^2 distribution with 3 (5) degrees of freedom.

2 Classical (frequentist) technique

2.1 Cartesian coordinates

The 4-dimensional cartesian parameter space is defined by the variables $\mathbf{z}_\pm = (x_\pm, y_\pm)$, where

$$\begin{aligned} x_\pm &\equiv \Re(r_{B\pm} e^{i\theta_\pm}) = r_{B\pm}\cos\theta_\pm \\ y_\pm &\equiv \Im(r_{B\pm} e^{i\theta_\pm}) = r_{B\pm}\sin\theta_\pm \end{aligned} \tag{3}$$

with $\theta_\pm = \delta \pm \gamma$. The choice of this particular basis is important because no physics boundaries have to be imposed to the fit variables. The consequence, as proved later, is the Gaussian behavior of the errors and the absence of biases in the fit results. On the contrary, the choice of the polar coordinates base,

$$(r_B\ ,\ \gamma\ ,\ \delta)\ , \tag{4}$$

even if it has one parameter less, it contains one parameter with a physics boundary ($r_B > 0$). In this case it is found a biased distribution for the r_B fit values, where the bias is larger for smaller values of r_B and smaller data sample size. In addition, cartesian coordinates are largely uncorrelated, while (r_B, γ, δ) are significantly correlated. The correlation matrix blocks for D^0K and $D^{*0}K$ modes obtained from the fit to the BlackDiamond data sample are shown in tables 1 and 2, respectively. As shown later on the basis of Toy MC studies, the only sizeable correlations appear for pairs (x_+, y_+) and (x_-, y_-) within a given B decay mode. This contribution will be taken later into account in the frequentist PDF. All the cross correlation terms between D^0K and $D^{*0}K$ samples are zero.

Moreover, the cartesian coordinates are sensitive to the direct *CP* violation in the $B^- \to D^{(*)0}K^-$ decay (and that with a simple Gaussian behavior). If we represent in the $(x_\pm, y_\pm)$ plane the results for $B^\pm$ decays, the distance of the two points d is

$$d \ = \ [(x_- - x_+)^2 + (y_- - y_+)^2]^{1/2} = 2r_B|\sin\gamma|\ . \tag{5}$$

A non null distance means evidence of direct *CP* violation.

Table 3 reports the $(x_\pm, y_\pm)$ nominal fit results on the BlackDiamond data sample, for the D^0K and $D^{*0}K$ decay modes. In Figure 1 are shown the 68.3% and 95% confidence-level contours in the $(x_\pm, y_\pm)$ cartesian fit parameter space for the two channels. The distance d is the length of the segment between the B^+ (circle dot) and B^- (rectangular dot). The statistical significance of the *CP* violation will be discussed later in section 2.5. Given the good Gaussian behavior of the cartesian parameters (see below), these contours have been obtained using the standard likelihood ratio method ($\Delta\mathcal{L}_{exp} = 0.5, 1.921$, for 68.3% and 95% confidence-level regions) [3].

From Toy MC studies, described in detail in Appendix A, residual distributions of the cartesian fit parameters space doesn't show any significant bias. The errors from the fit are well calculated, pulls (residuals normalized to the fit errors) have $\sigma = 1$ within the errors for all the fit variables and means are consistent with zero. For this study we have used a set of about 2K Toy MC experiments corresponding to the nominal data results (i.e. the generated $x_\pm$ and $y_\pm$ values are those found in the nominal fit, table 3). The linearity of the $(x_\pm, y_\pm)$ fit parameters together with the stability of their corresponding rms' (σ_{x_+}, σ_{y_+}, σ_{x_-}, and σ_{y_-}) versus the generated parameter values are demonstrated in figures 2 and 3, for the D^0K and $D^{*0}K$ samples respectively (error bars indicate

Observable	x_-	y_-	x_+	y_+
x_-	1	2.5×10^{-2}	9.4×10^{-5}	-3.0×10^{-5}
y_-		1	-1.8×10^{-4}	-2.3×10^{-4}
x_+			1	6.0×10^{-2}

Table 1: *Correlation matrix for $(x_\pm, y_\pm)$ cartesian coordinates, for the D^0K decay mode.*

Observable	x_-	y_-	x_+	y_+
x_-	1	-1.7×10^{-1}	-6.3×10^{-3}	3.6×10^{-3}
y_-		1	-5.7×10^{-3}	2.6×10^{-3}
x_+			1	-2.7×10^{-1}

Table 2: *Correlation matrix for $(x^*_\pm, y^*_\pm)$ cartesian coordinates, for the $D^{*0}K$ decay mode.*

Observable	D^0K	$D^{*0}K$
x_-	$0.0772^{+0.0688}_{-0.0708}$ [± 0.0692]	$-0.1306^{+0.0940}_{-0.0935}$ [± 0.0934]
y_-	$0.0635^{+0.0953}_{-0.0888}$ [± 0.0919]	$-0.1433^{+0.1064}_{-0.1059}$ [± 0.1049]
x_+	$-0.1287^{+0.0701}_{-0.0704}$ [± 0.0703]	$0.1397^{+0.0941}_{-0.0943}$ [± 0.0926]
y_+	$0.0186^{+0.0762}_{-0.0814}$ [± 0.0787]	$0.0131^{+0.1183}_{-0.1201}$ [± 0.1195]

Table 3: *Fit results for $(x_\pm, y_\pm)$ cartesian coordinates, for the D^0K and $D^{*0}K$ decay modes. The values inside square brackets are the quadratic (Gaussian) errors calculated from the fit covariance matrix.*

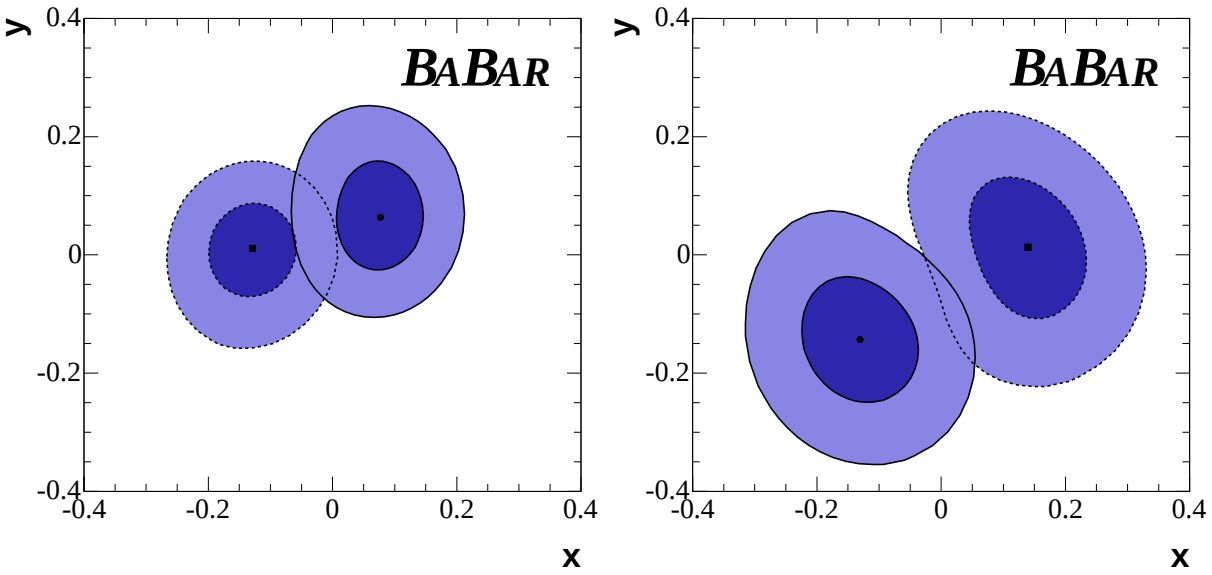

Figure 1: *68.3% (dark blue) and 95% (bright blue) confidence-level countours in the* $(x_\pm, y_\pm)$ *cartesian fit parameter space for* D^0K *(left) and* $D^{*0}K$ *(right). Solid (dotted) contours are for* B^- *(*B^+*) decays. Given the good Gaussian behavior of the cartesian parameters, these contours have been obtained using the standard likelihood ratio method (*$\Delta\mathcal{L}_{exp} = 0.5, 1.921$*) [3].*

the rms of the distribution at each generated point). These figures have been produced with 20K Toy MC experiments with truth $(x_\pm, y_\pm)$ values obtained by generating randomly r_B and the weak and strong phases, in the ranges $[0, 0.3]$, $[-180°, 180°]$ and $[0, 360°]$, respectively. Using the same experiments we have also studied the stability of the rms of the residual and pull distributions in bins of the truth r_B value, as shown in Appendix A. From both studies we observe that the rms values are stable in the wide range of truth values within a precision of $< 10\%$. These results will be used in the parametrization of the frequentist PDF, as described below.

2.2 Description of the method

Once we have demonstrated the Gaussian and linearity behavior of the cartesian fit parameter space, we can construct an analytical parameterization of the PDF. The 4-dimensional PDF is written as

$$\begin{aligned}\frac{d^4P}{d^2\mathbf{z}_+ d^2\mathbf{z}_-}(\mathbf{z}_+, \mathbf{z}_-|\mathbf{p}^{\rm t}) &= G_2\left(\mathbf{z}_+; r_B^t\cos(\delta^t+\gamma^t), r_B^t\sin(\delta^t+\gamma^t), \sigma_{x_+}, \sigma_{y_+}, \rho_+\right) \times \\ &\quad G_2\left(\mathbf{z}_-; r_B^t\cos(\delta^t-\gamma^t), r_B^t\sin(\delta^t-\gamma^t), \sigma_{x_-}, \sigma_{y_-}, \rho_-\right) \qquad (6)\end{aligned}$$

where

$$G_2\left(\mathbf{z}; \mu_x, \mu_y, \sigma_x, \sigma_y, \rho\right) = \frac{1}{2\pi\sigma_x\sigma_y\sqrt{1-\rho^2}} e^{-\frac{1}{2(1-\rho^2)}\left[\frac{(x-\mu_x)^2}{\sigma_x^2}+\frac{(y-\mu_y)^2}{\sigma_y^2}-\frac{2\rho(x-\mu_x)(y-\mu_y)}{\sigma_x\sigma_y}\right]} \qquad (7)$$

and $\mathbf{z}_\pm = (x_\pm, y_\pm)$ and $\mathbf{p} = (r_B, \gamma, \delta)$. The vectors $\mathbf{z}_\pm^{\rm t}$ and $\mathbf{p}^{\rm t}$, defined equivalently to $\mathbf{z}_\pm$ and $\mathbf{p}$ respectively, are the corresponding parameters in the truth parameter space. The Gaussian

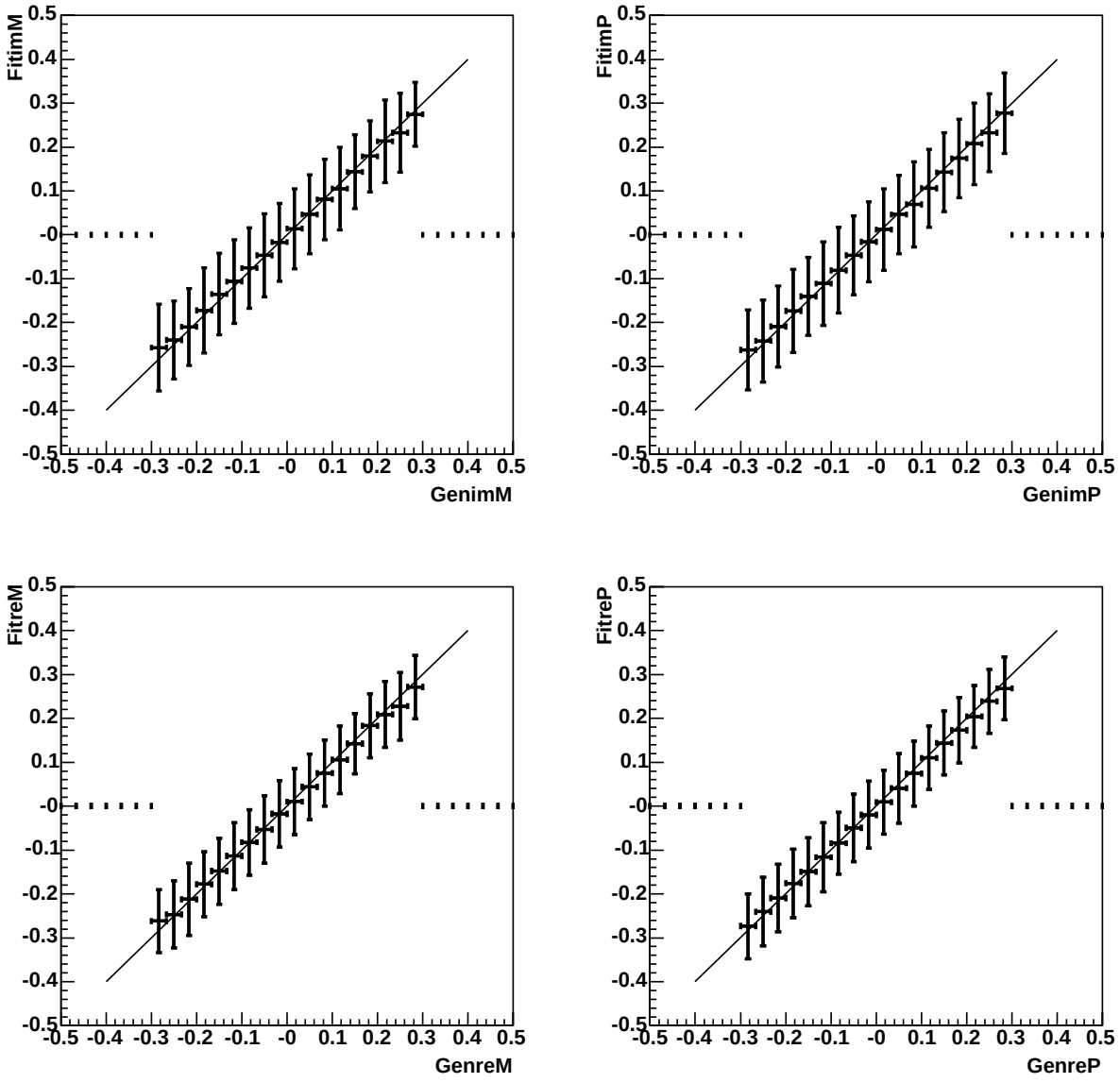

Figure 2: *Linearity of the* $(x_{\pm}, y_{\pm})$ *cartesian fit parameter space, for the* D^0K *mode. The truth (generated) values of* $(x_{\pm}, y_{\pm})$ *have been obtained by generating randomly* r_B *and the weak and strong phases.* r_B *was generated in the range* $[0, 0.3]$*. Error bars indicate the rms of the distribution at each generated point.*

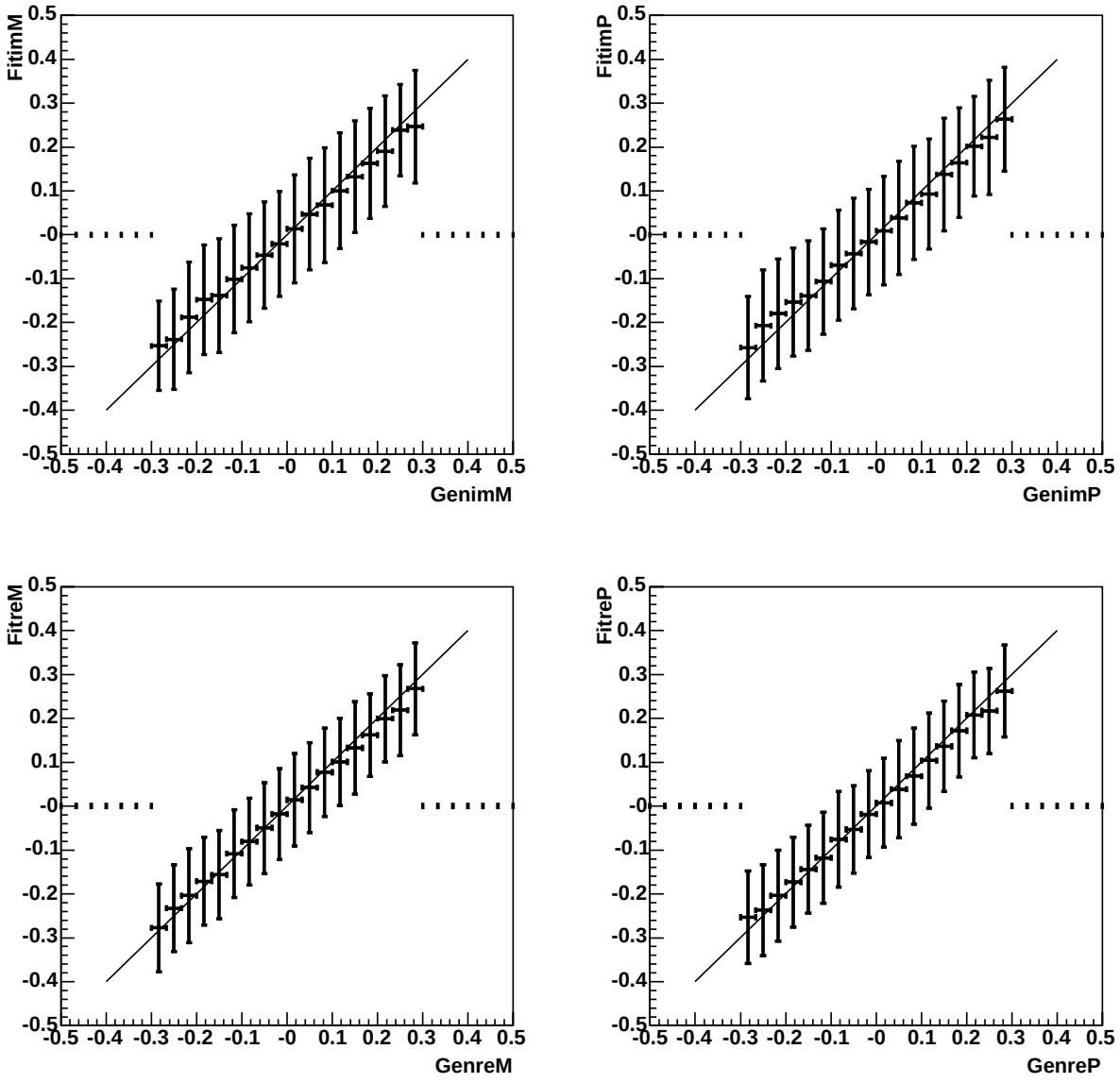

Figure 3: *Linearity of the* $(x_\pm, y_\pm)$ *cartesian fit parameter space, for the* $D^{*0}K$ *mode. The truth (generated) values of* $(x_\pm, y_\pm)$ *have been obtained by generating randomly* r_B *and the weak and strong phases.* r_B *was generated in the range* $[0, 0.3]$*. Error bars indicate the rms of the distribution at each generated point.*

widths ($\sigma_{x_\pm}$, $\sigma_{y_\pm}$) and the correlations $\rho_\pm$ (all the other correlations are neglected) distributions can obtained either from the nominal full experimental likelihood $\mathcal{L}_{exp}$ Toy MC experiments or from the fit to the data sample itself, since the agreement with the values found in data is very good, as shown in figures 30, 31 and 32 in Appendix A. Given this good agreement and in order to take into account the goodness of the fit to the data sample (i.e. good or bad luck of the data sample single experiment), we will use in the above PDF the values of the widths and correlations found in the data fit, which were summarized in tables 3, 1 and 2.

Once we have constructed and justified the PDF of the fit parameters as a function of the true parameters, the technical procedure to construct 3-dimensional confidence regions and their 1- and 2-dimensional is as follows. The confidence level $1-\alpha$ for each set of true parameters $\mathbf{p}^{\rm t}$ is calculated as

$$\alpha(\mathbf{p}^{\rm t}) \;\; = \;\; \int_D \frac{d^4P}{d^2\mathbf{z}_+ d^2\mathbf{z}_-}(\mathbf{z}_+,\mathbf{z}_-|\mathbf{p}^{\rm t}) d^2\mathbf{z}_+ d^2\mathbf{z}_- \;\; , \tag{8}$$

where the integration domain D (the confidence region) is given by the condition

$$\frac{d^4P}{d^2\mathbf{z}_+ d^2\mathbf{z}_-}(\mathbf{z}_+,\mathbf{z}_-|\mathbf{p}^{\rm t}) \geq \frac{d^4P}{d^2\mathbf{z}_+ d^2\mathbf{z}_-}(\mathbf{z}_+^{\rm data},\mathbf{z}_-^{\rm data}|\mathbf{p}^{\rm t}) \;\; , \tag{9}$$

i.e. it includes all points in the fit parameter space closer to the truth point than the data point. The values of $\mathbf{z}_\pm^{\rm data}$ are those given in table 3. To construct the 3-dimensional confidence region ($\mathbf{p}^{\rm t}$ space) we generate randomly a large set (10^9) of points $\mathbf{p}^{\rm t} \equiv (r_B^t, \gamma^t, \delta^t)$, in the ranges $[0, 0.4]$, $[-180^\circ, 180^\circ]$ and $[0, 360^\circ]$. For each generated point $\mathbf{p}^{\rm t}$ the integral $\alpha(\mathbf{p}^{\rm t})$ is evaluated according to equations (8) and (9). If we are interested in building a 3-dimensional region of joint probability $1-\alpha_0$, then we select only those points for which $\alpha(\mathbf{p}^{\rm t}) \leq \alpha_0$. The 2-dimensional and 1-dimensional contours are then built by projecting the 3-dimensional joint probability regions. The values $\alpha_0 = 0.19875, 0.72092$ correspond to the 1 and 1.96 standard deviation 3-dimensional ellipsoids, thus the 1-dimensional projections represent the 1 and 1.96 standard deviations of each individual parameter[2], regardless the other parameters[3]. This procedure results in a confidence domain with the minimum possible area and so has maximum power to exclude alternative hypotheses. The integral (8) with the contour condition given by Eq. (9) can be evaluated numerically, but an analytical evaluation is also possible by performing a change of variable to 4-dimensional hyperspheric coordinates, with the subsequent gain in CPU (many orders of magnitude) and precision.

The Neyman's freedom to define the likelihood ordering offers also the possibility to use alternatively the likelihood ordering proposed in [5] instead of that given in Eq. (9). In this paper it is raised the issue of undercoverage produced by the usual orderings, like the one used here, when measured parameters are bounded by physical limits. In addition to the alternative ordering proposed by Feldman and Cousins, a possible way out (also pointed out in their paper) is to allow the measured parameters to take unphysical values. This requires knowning the PDF for non-physical values, which often raises conceptual problems. However, we should stress here that we are free of this problem since our fit parameter space (cartesian coordinates) is not bounded. Obviously, this does not imply that our ordering choice and that of Feldman-Cousins provide exactly the same confidence regions (this is the inherent freedom to the Neyman's definition) but both provide regions with the correct statistical coverage. The correct coverage provided by our method and particular ordering is demonstrated in section 2.6.

[2] 1.96σ corresponds to a 95% probability content for the case of a 1-dimensional Gaussian distribution [3].

[3] These values of α_0 are the cumulative (upper) integral of a χ^2 probability distribution for $\chi^2 = 1^2, 1.96^2$ and $\nu = 3$ degrees of freedom [3].

As an additional cross-check we have verified that the 68.3% confidence level interval for a point in the true parameter space with $r_B^t = 0$ (null point, i.e. $\mathbf{z}_\pm^{\rm t} = \mathbf{0}$) contains $r_B^t = 0$ (see Appendix B). This check is relevant to verify that the method intrinsically accounts for the r_B bias.

2.3 1- and 2-dimensional projections of confidence regions for D^0K and $D^{*0}K$

Applying this procedure separately to D^0K and $D^{*0}K$, and projecting in 1 and 2 dimensions we obtain the projections of the 3-dimensional regions of $1-\alpha_0$ joint probability. Figures 4 and 5 show the 2-dimensional projections of the the 19.9% (dark blue) and 72.1% (bright blue) confidence-level 3-dimensional regions for the D^0K and $D^{*0}K$ modes. Similarly, figures 6 and 7 show the 1-dimensional projections, which correspond to 1 and 1.96 sigma standard deviation of each single parameter, regardless the values of the others. In the 1-dimensional projections we also show the projection of the PDF. Notice that both the 2- and 1-dimensional projections show the $\pm 180^\circ$ ambiguity in $\gamma^{(*)}$ and $\delta^{(*)}$. The probability density functions for r_B and r_B^* show clearly the non-Gaussian behavior we expect from Toy MC, as well as the poor sensitivity to small values. Table 4 reports numerically the one dimensional 1σ and 1.96σ intervals[4]. The results include the intrinsic two fold ambiguity for $\gamma^{(*)}$ and $\delta^{(*)}$.

Parameter	1σ	1.96σ
r_B	[0.051,0.184]	[0,0.238]
γ	[33,108] [213,288]	–
δ	[67,142] [247,322]	–
r_B^*	[0.090],0.248]	[0.027,0.318]
γ^*	[36,106] [216,286]	[11,140] [191,320]
δ^*	[262,332] [82,152]	[234,363] [54,183]

Table 4: *The 1σ (1.96σ) intervals for r_B, δ, γ (D^0K) and r_B^*, γ^* and δ^* ($D^{*0}K$). For γ and δ the ± 180 degree solution is also indicated.*

2.4 Combination of D^0K and $D^{*0}K$ decay modes

We have combined the two event samples, D^0K and $D^{*0}K$, in order to obtain a more accurate measurement of γ. The method we have used for the combination of the results is identical to that used for each B decay mode separately, but now we have five true parameters $\mathbf{p}^{\rm t}= (\gamma^t, r_B^t, \delta^t, r_B^{*t}, \delta^{*t})$ and an 8-dimensional cartesian space for the measured parameters $(\mathbf{z}_\pm, \mathbf{z}_\pm^*) = (x_\pm, y_\pm, x_\pm^*, y_\pm^*)$. The PDF in this case reads

$$\begin{aligned}\frac{d^8P}{d^2\mathbf{z}_+ d^2\mathbf{z}_- d^2\mathbf{z}_+^* d^2\mathbf{z}_-^*}(\mathbf{z}_+, \mathbf{z}_-, \mathbf{z}_+^*, \mathbf{z}_-^* | \mathbf{p}^{\rm t}) &= \frac{d^4P}{d^2\mathbf{z}_+ d^2\mathbf{z}_-}(\mathbf{z}_+, \mathbf{z}_- | r_B^t, \gamma^t, \delta^t) \times \\ &\quad \frac{d^4P}{d^2\mathbf{z}_+^* d^2\mathbf{z}_-^*}(\mathbf{z}_+^*, \mathbf{z}_-^* | r_B^{*t}, \gamma^t, \delta^{*t}) \ . \end{aligned} \tag{10}$$

The confidence level $1-\alpha$ for each set of true parameters $\mathbf{p}^{\rm t}$ is now calculated as

[4]The numerical confidence intervals have been obtained using 10^9 points and an step variation (precision) of 0.0002 on r_B and 0.1° on the angles, while for the 2- and 1-dimensional figures a poorer precision of 10^7 points and an step variation of 0.004 and 3° is enough (a better, publication quality could be obtained with 5×10^7 points and an step variation of 0.001 and 1°).

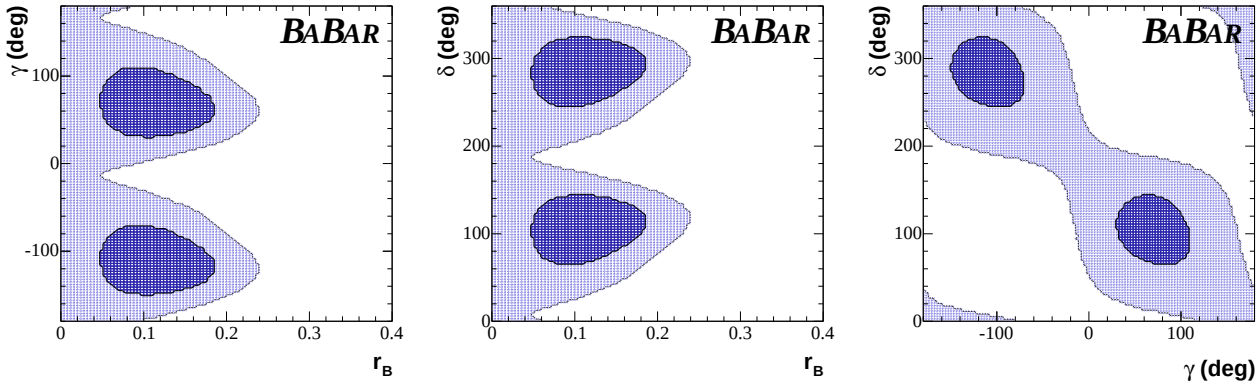

Figure 4: *2-dimensional projections of the 19.9% (dark blue) and 72.1% (bright blue) confidence-level 3-dimensional regions for the D^0K mode.*

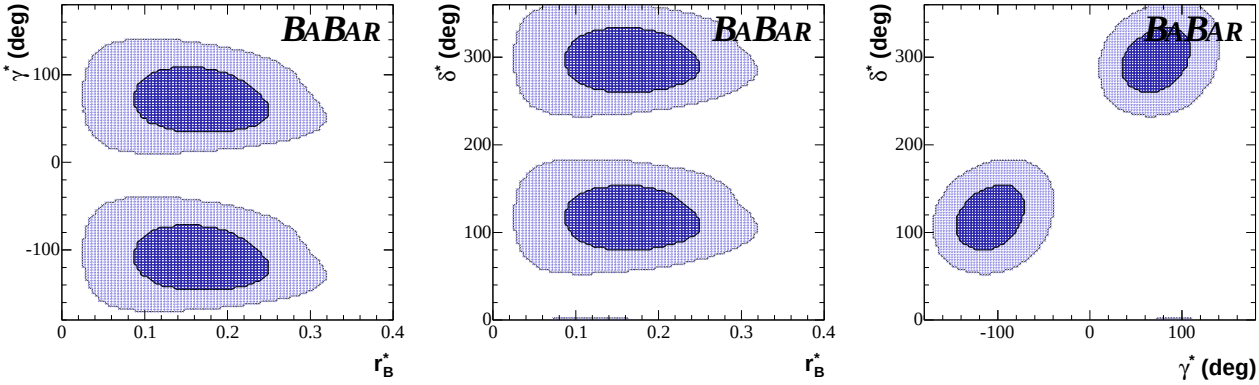

Figure 5: *2-dimensional projections of the 19.9% (dark blue) and 72.1% (bright blue) confidence-level 3-dimensional regions for the $D^{*0}K$ mode.*

$$\alpha(\mathbf{p}^{\rm t}) \;=\; \int_D \frac{d^8P}{d^2\mathbf{z}_+ d^2\mathbf{z}_- d^2\mathbf{z}_+^* d^2\mathbf{z}_-^*}(\mathbf{z}_+,\mathbf{z}_-,\mathbf{z}_+^*,\mathbf{z}_-^*|\mathbf{p}^{\rm t}) d^2\mathbf{z}_+ d^2\mathbf{z}_- d^2\mathbf{z}_+^* d^2\mathbf{z}_-^* \;, \tag{11}$$

where the integration domain D (the confidence region) is given by the condition

$$\frac{d^8P}{d^2\mathbf{z}_+ d^2\mathbf{z}_- d^2\mathbf{z}_+^* d^2\mathbf{z}_-^*}(\mathbf{z}_+,\mathbf{z}_-,\mathbf{z}_+^*,\mathbf{z}_-^*|\mathbf{p}^{\rm t}) \geq \frac{d^8P}{d^2\mathbf{z}_+ d^2\mathbf{z}_- d^2\mathbf{z}_+^* d^2\mathbf{z}_-^*}(\mathbf{z}_+^{\rm data},\mathbf{z}_-^{\rm data},\mathbf{z}_+^{*\ {\rm data}},\mathbf{z}_-^{*\ {\rm data}}|\mathbf{p}^{\rm t}) \;. \tag{12}$$

The 5-dimensional confidence region in $\mathbf{p}^{\rm t}$ space is constructed by generating a large number (10^{10}) of points $\mathbf{p}^{\rm t} \equiv (r_B^t, \gamma^t, \delta^t, r_B^{t\,*}, \delta^*)$, in the ranges $[0, 0.4]$, $[-180°, 180°]$, $[0, 360°]$, $[0, 0.4]$, and $[0, 360°]$, respectively, and selecting the points for which $\alpha(\mathbf{p}^{\rm t}) \leq \alpha_0 = 0.03743, 0.42756$. These values α_0 correspond to the 1 and 1.96 standard deviation 5-dimensional ellipsoids, thus the 1-dimensional projections represent the 1 and 1.96 standard deviations of each individual parameter, regardless the other parameters [5]. As before, the 2- and 1-dimensional contours are then built

[5] These values of α_0 are the cumulative (upper) integral of a χ^2 probability distribution for $\chi^2 = 1^2, 1.96^2$ and $\nu = 5$ degrees of freedom [3].

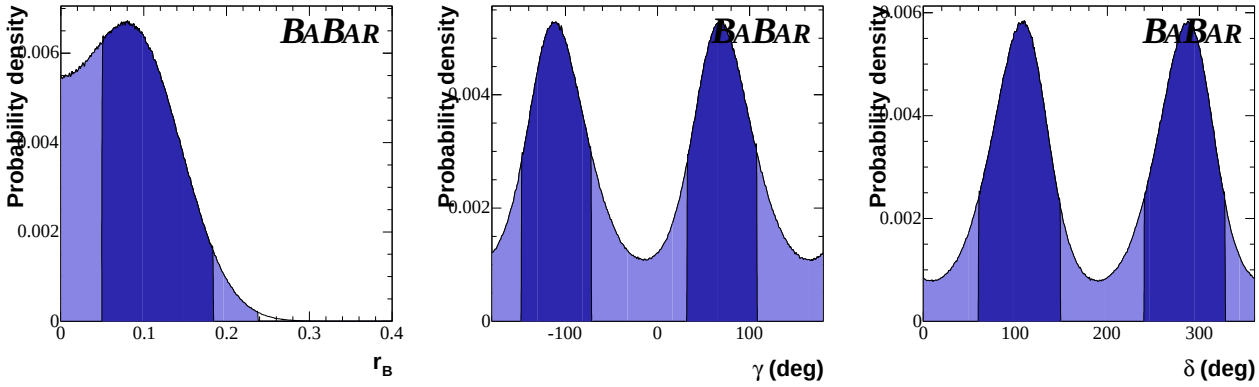

Figure 6: *Probability density functions for r_B, γ and δ together with the 1-dimensional projections of the 19.9% (dark blue) and 72.1% (bright blue) confidence-level 3-dimensional regions for the D^0K mode.*

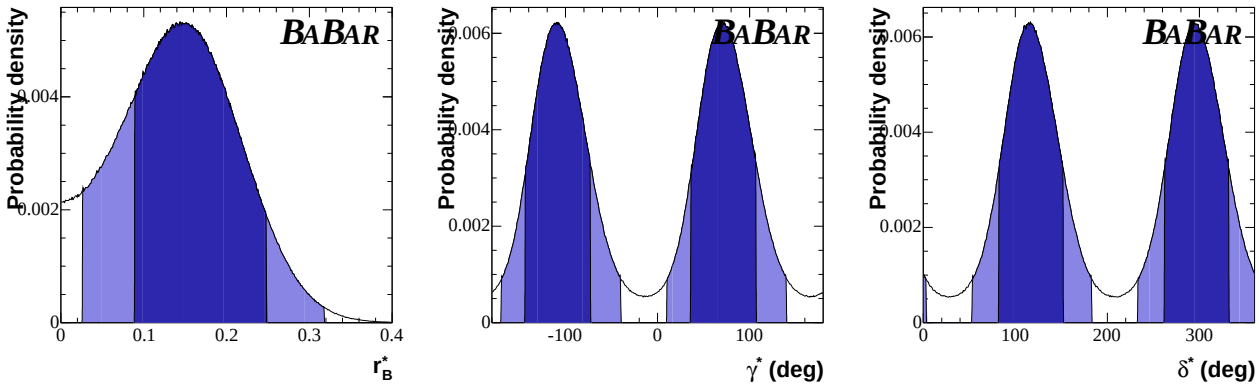

Figure 7: *Probability density functions for ${r_B}^*$, γ and δ^* together with the 1-dimensional projections of the 19.9% (dark blue) and 72.1% (bright blue) confidence-level 3-dimensional regions for the $D^{*0}K$ mode.*

by projecting the 5-dimensional joint probability regions. Figures 8 and 9 show the 2-dimensional projections of the 3.7% (dark blue) and 42.8% (bright blue) confidence-level 5-dimensional regions for D^0K and $D^{*0}K$ modes (γ is common). The corresponding 1-dimensional projections, together with the PDF projections, are shown in figure 10. Notice that both the 2- and 1-dimensional projections show the $\pm 180^\circ$ ambiguity in γ and $\delta^{(*)}$.

Table 5 reports numerically the 1-dimensional 1σ and 1.96σ intervals[6]. The results include the intrinsic two fold ambiguity for γ and $\delta^{(*)}$. In the last column of the table we also report central values of the true parameters with 1σ errors. The central values for the true parameters are estimated as the mean value of the interval (statistical only). The central value and one standard deviation (which corresponds to the 3.7% confidence level region for the case of a 5-dimensional

[6]The numerical confidence intervals have been obtained using 10^10 points and an step variation (precision) of 0.0002 on r_B and 0.1° on the angles, while for the 2- and 1-dimensional figures a poorer precision of 10^7 points and an step variation of 0.004 and 3° is enough (a better, publication quality could be obtained with 5×10^7 points and an step variation of 0.001 and 1°).

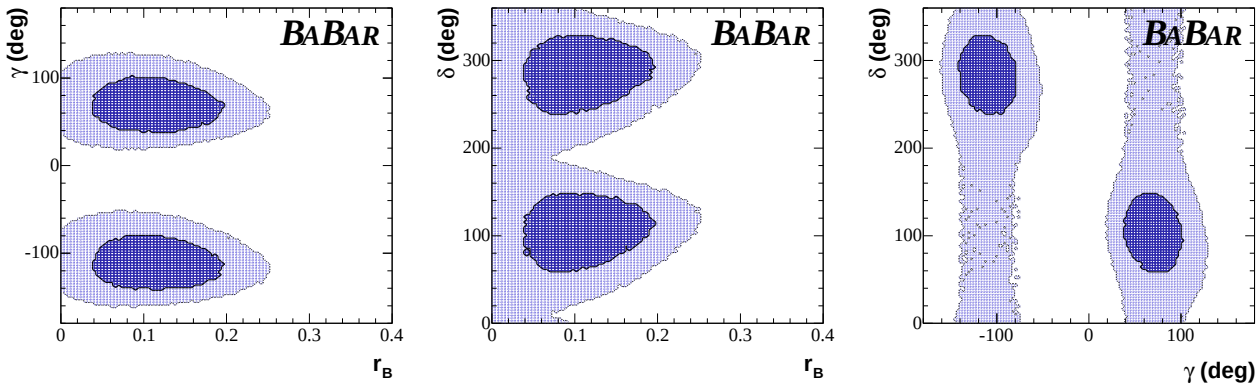

Figure 8: *2-dimensional projections of the 3.7% (dark blue) and 42.8% (bright blue) confidence-level 5-dimensional regions for the D^0K - $D^{*0}K$ combined mode. The r_B and δ variables are for the D^0K decay sample.*

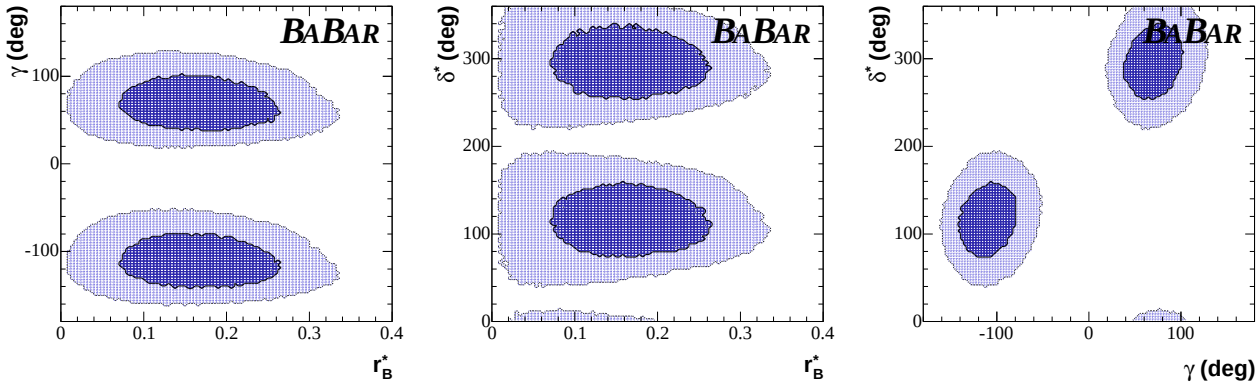

Figure 9: *2-dimensional projections of the 3.7% (dark blue) and 42.8% (bright blue) confidence-level 5-dimensional regions for the D^0K - $D^{*0}K$ combined mode. The $r_B{}^*$ and δ^* variables are for the $D^{*0}K$ decay sample.*

Gaussian distribution) for γ is therefore $\gamma = (70 \pm 31)^\circ$, while the 1.96 standard deviation interval (which corresponds to the 42.8% confidence level region for a 5-dimensional Gaussian distribution) is $20^\circ < \gamma < 128^\circ$ ($200^\circ < \gamma < 308^\circ$).

2.5 Significance of *CP* violation

The significance of *CP* violation can be determined by finding the confidence level $1 - \alpha_{\not CP}$ for the most probable *CP* conserving point $\mathbf{p}^{\rm t}_{CP}$, i.e. the $\mathbf{p}^{\rm t}$ point with $r_B^t = 0$ or $\gamma^t = 0$,

$$\mathbf{p}^{\rm t}_{CP} = \{\mathbf{p}^{\rm t} | \mathbf{p}^{\rm t} = (r_B^t = 0, \gamma^t, \delta^t) \text{ or } \mathbf{p}^{\rm t} = (r_B^t, \gamma^t = 0, \delta^t)\} \ . \tag{13}$$

for which $\alpha(\mathbf{p}^{\rm t})$ is minimal. In this way, $1 - \alpha_{\not CP}$ represents the *CP* conservation confidence level, and therefore $\alpha_{\not CP}$ represents the *CP* violation confidence level (or significance of *CP* violation).

In the case of the combined measurement of γ we can evaluate the *CP* significance as follows

$$\mathbf{p}^{\rm t}_{CP} = \{\mathbf{p}^{\rm t} | \mathbf{p}^{\rm t} = (r_B^t = 0, r_B^{*t} = 0, \gamma^t, \delta^t, \delta^{*t}) \text{ or } \mathbf{p}^{\rm t} = (r_B^t, r_B^{*t}, \gamma^t = 0, \delta^t, \delta^{*t})\} \ . \tag{14}$$

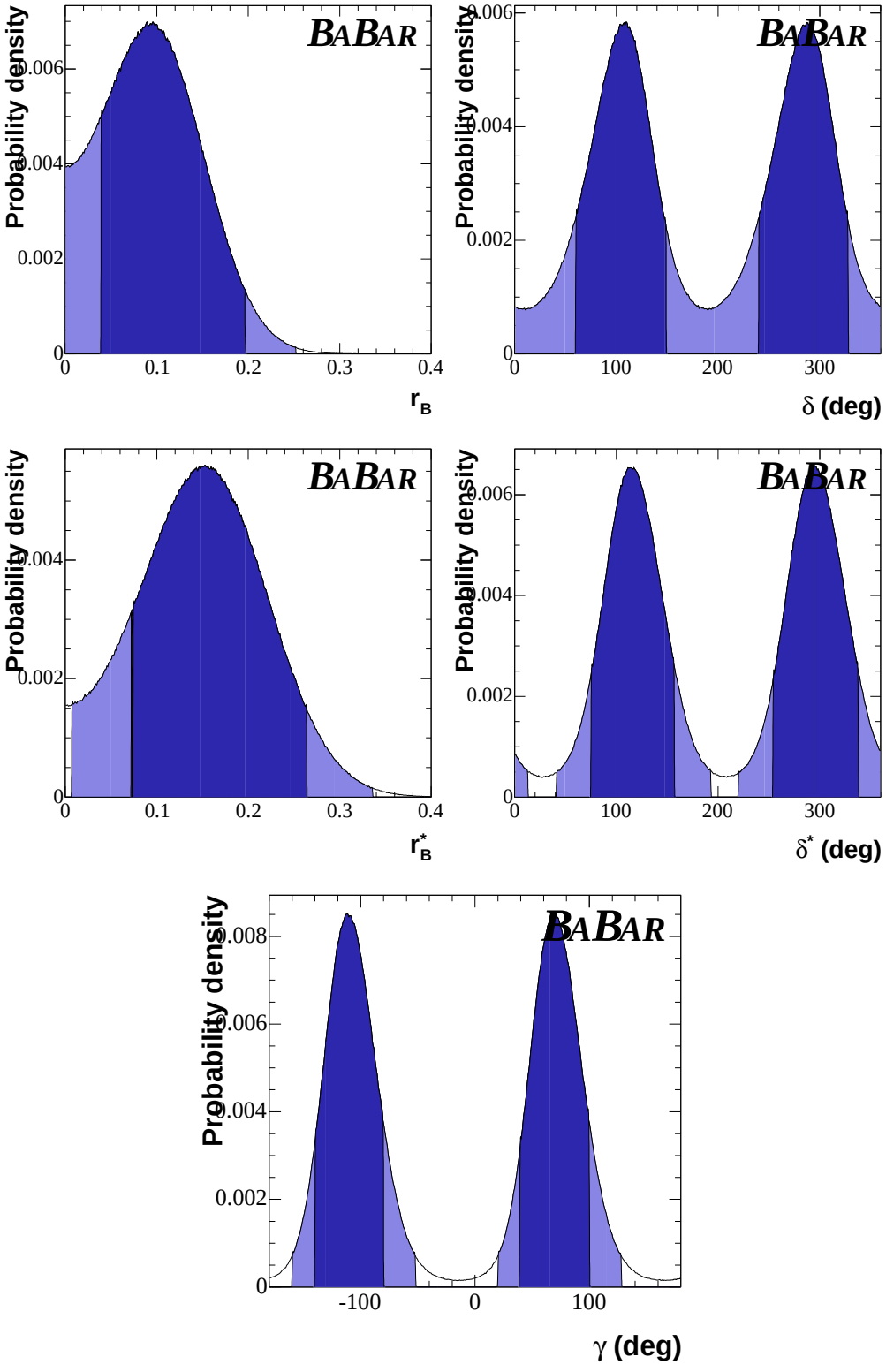

Figure 10: *Probability density functions for r_B, δ, $r_B{}^*$, δ^* and γ together with the 1-dimensional projections of the 3.7% (dark blue) and 42.8% (bright blue) confidence-level 5-dimensional regions for the D^0K - $D^{*0}K$ combination.*

Parameter	1σ	1.96σ	Central value with error (1σ)
γ	[39,101] [219,281]	[20,128] [200,308]	70 ± 31
r_B	[0.040,0.196]	[0,0.253]	0.118 ± 0.079
r_B^*	[0.073],0.265]	[0.007,0.336]	0.169 ± 0.096
δ	[59,149] [239,329]	–	104 ± 45
δ^*	[255,338] [75,158]	[220,374] [40,194]	296 ± 41

Table 5: *The 1σ (1.96σ) D^0K-$D^{*0}K$ combined intervals for r_B, $r_B{}^*$, δ, δ^*, and γ (angles are in degree). In the last column the central values with 1σ errors are also reported. For the γ, δ and δ^* intervals the ± 180 degree solution is also indicated.*

For the D^0K we have $\alpha_{\not{CP}} = 0.655$ in $\mathbf{p}^{\rm t}$=(r_B^t,γ^t,δ^t)=(0.043,0°,124°), for the $D^{*0}K$ we have $\alpha_{\not{CP}} = 0.828$ in $\mathbf{p}^{\rm t}$=(r_B^{*t},γ^t,δ^{*t})=(0.070,0°, 280°), while for the combined measurement we have $\alpha_{\not{CP}} = 0.791$ in $\mathbf{p}^{\rm t}$=(r_B^t,γ^t,δ^t,r_B^{*t},δ^{*t})=(0.044,0°,123°,0.073,279°). We quote *CP* violation in the D^0K at 65.5% CL, in the $D^{*0}K$ at 82.8% CL and in the combined measurement at the 79.1% CL. These confidence levels correspond to the 1.82, 2.24, and 2.68 standard deviation ellipsoids.

2.6 Coverage test with the experimental likelihood

A simple and powerful check that the whole procedure has been applied and implemented correctly, including the (very good) simplifications made when constructing the analytical forms of the frequentist PDFs, Eqs. (6) and (10), is to check the coverage (in a frequentist sense) given by the estimated confidence regions using the (full) experimental likelihood $\mathcal{L}_{exp}$. The test makes use of the frequentist definition of coverage, as given in section 1: a region with confidence level $1-\alpha_0$ will contain the unknown true point a fraction $1-\alpha_0$ of the experiments, or in other words, if the experiment is carried out many times, a fraction $1-\alpha_0$ of those experiments will find the measured point within the given confidence region. Following this definition, the procedure was the following. About 20K Toy MC experiments tuned to the data were generated with truth values of r_B, γ, δ, $r_B{}^*$ and δ^* as obtained after applying the frequentist method (central values), as given in Table 5. These values represent in fact the vector of true parameters, $\mathbf{p}^{\rm t} = (r_B^t, \gamma^t, \delta^t, r_B^{*t}, \delta^{*t})$. Each experiment was then fit in cartesian coordinates, obtaining a set of $(x_\pm^i, y_\pm^i)$, $(x_\pm^{*i}, y_\pm^{*i})$ values from which the confidence level $1-\alpha(\mathbf{p}^{\rm t})$ was calculated using Eqs. (11) and (12), where now the *data* point is substituted by the *Toy MC experiment* point. If the procedure provides the correct coverage then the fraction of Toy MC experiments verifying $\alpha(\mathbf{p}^{\rm t}) \leq \alpha_0$ should be just α_0 (or consistent with it).

The $\alpha_0 = 3.74\%$ (42.76%) 5-dimensional confidence-level coverage is $3.75 \pm 0.14\%$ ($40.4 \pm 0.5\%$), where the error is due to the limited amount of Toy MC experiments. The discrepancy at the 5 sigma level (5.5%) for the 1.96σ coverage is due to small deviations of the experimental likelihood $\mathcal{L}_{exp}$ with respect to the perfect Gaussian behavior and the assumption of the stability of the widths (σ_{x_+}, σ_{y_+}, σ_{x_-}, and σ_{y_-}) over the whole range of the parameters, known to be true at $< 10\%$ level for parameters far away from those found in the nominal data fit (this explains the perfect agreement at 1σ level and the small difference at 1.96σ). The confidence level corresponding to $\alpha_0 = 40.4\%$ translates into a 1.92σ ellipsoid, to be compared to the nominal 1.96σ (in terms of 1-dimensional Gaussian probability content this corresponds to 94.5%, to be compared to the nominal 95%). Therefore the discrepancy is negligible. The coverage as a function of the value of α_0 in bins of size 0.1 is shown in figure 11. Within errors, the coverage is correct for all the possible confidence level values.

The coverage check has been repeated by changing the truth value of r_B and r_B^* by $\pm 1\sigma$

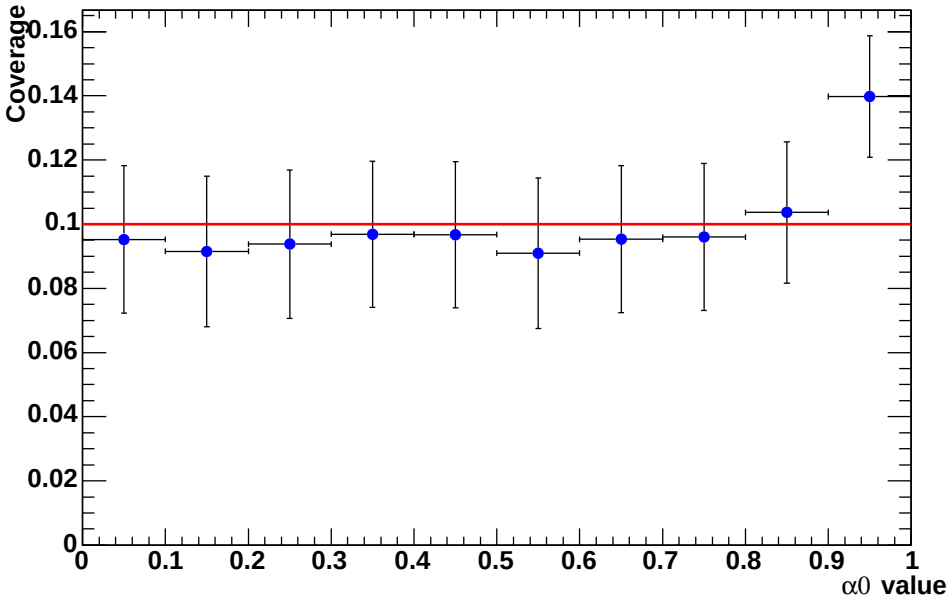

Figure 11: *Distribution of the α_0 value in the ToyMC experimental likelihood (coverage) for the central values of truth r_B and r_B^* values (table 5). The red line represents the perfect coverage case, blue points are the coverage value from the ToyMC experiments for each α_0 bin of size 0.1. The error bars are due to the limited statistics of experiments (20K). Within errors, the coverage is correct for all the possible confidence level values.*

(according to the last column of table 5), keeping the same values for the phases. Moving r_B and r_B^* is enough for the purpose of this check since what we want to study is any potential change in the coverage by the scaling of the cartesian coordinates. A total of 10K experiments were generated for each of these points. The $\alpha_0 = 3.74\%$ (42.76%) 5-dimensional confidence-level coverage for the lower 1σ bound is $4.1 \pm 0.2\%$ and for the upper bound is $3.6 \pm 0.2\%$. The coverage as a function of the value of α_0 in bins of size 0.1 for these two points is also shown in figure 12. Again, taking into account the statistical errors, the coverage is correct for all the possible confidence level values.

Finally, as a sanity check, we used the same Toy MC experiments to check directly the 1-dimensional coverage provided by the cartesian coordinates $(x_\pm, y_\pm)$ and $(x_\pm^*, y_\pm^*)$, which turn to be perfectly consistent with 68.3% (95%) with an error from the limited number of Toy MC experiments of 0.006 (0.007).

2.7 *CP* test with the $D^0\pi$ and $D^{*0}\pi$ events

The *CP* analysis has also been performed with $D^0\pi$ and $D^{*0}\pi$ events in exactly the same way as it has been done for the D^0K and $D^{*0}K$ samples. The goal of this check is to verify whether the results are consistent with the expectation that *CP* violating effects are much smaller than for D^0K and $D^{*0}K$ events ($r_B{}^{(*)}$ values are expected to be of order 0.007).

Table 6 reports the $(x_\pm, y_\pm)$ *CP* fit results on the BlackDiamond data sample, for the $D^0\pi$ and $D^{*0}\pi$ decay modes. The corresponding correlation matrix blocks obtained from the fit are shown in tables 7 and 8, respectively.

Figures 13 and 14 show the 2-dimensional projections of the 19.9% (dark blue) and 72.1% (bright blue) confidence-level 3-dimensional regions for the $D^0\pi$ and $D^{*0}\pi$ modes. Similarly, figures 15 and 16 show the 1-dimensional projections, which correspond to 1 and 1.96 sigma standard deviation of each single parameter, regardless the values of the others. Table 9 reports numerically the one dimensional 1σ and 1.96σ intervals.

We have also combined the two event samples, $D^0\pi$ and $D^{*0}\pi$. Figures 17 and 18 show the 2-dimensional projections of the 3.7% (dark blue) and 42.8% (bright blue) confidence-level 5-dimensional regions for $D^0\pi$ and $D^{*0}\pi$ modes (γ is common). The corresponding 1-dimensional projections, together with the PDF projections, are shown in figure 19. Table 10 reports numerically the 1-dimensional 1σ and 1.96σ intervals. In the last column of the table we also report central values of the true parameters with 1σ errors. The central values for the true parameters are estimated as the mean value of the interval (statistical only). The results for ${r_B}^{(*)}$ are consistent with the expectations. Although the current $D\pi$ data does not constraint at 1.96σ level the weak and strong phases (the sensitivity is just at the frontier, as seen in the previous figures), the 1σ γ constraint is similar and consistent with what we obtained with the DK samples. On the other hand, looking at the 2-dimensional projections of the joint probability ellipsoids as well as to the PDF projections is it obvious that there is some interesting sensitivity to γ. This could be exploited in the future to perform a DK-$D\pi$ combined frequentist analysis to improve the statistical power on γ (this will require more careful studies of the $D^0\pi$ and $D^{*0}\pi$ background composition as well as the evaluation of the $D\pi$ *CP* systematics). As a new check that the sensitivity we observe in $D\pi$ events is not an artifact we have performed a null $D^0\pi$ test, as described in Appendix C. The significance of *CP* violation is $\alpha_{\not{CP}} = 0.004$ for $D^0\pi$, $\alpha_{\not{CP}} = 0.649$ for $D^{*0}\pi$, and $\alpha_{\not{CP}} = 0.204$ for the $D^0\pi$-$D^{*0}\pi$ combination.

Observable	D^0K	$D^{*0}K$
x_-	-0.0157 ± 0.0167	0.0608 ± 0.0288
y_-	-0.0135 ± 0.0200	0.0209 ± 0.0371
x_+	-0.0061 ± 0.0186	-0.0242 ± 0.0283
y_+	-0.0186 ± 0.0196	0.0205 ± 0.0323

Table 6: *Fit results for $(x_\pm, y_\pm)$ cartesian coordinates, for the $D^0\pi$ and $D^{*0}\pi$ decay modes.*

Observable	x_-	y_-	x_+	y_+
x_-	1	6.8×10^{-2}	6.1×10^{-4}	1.3×10^{-5}
y_-		1	-8.0×10^{-4}	2.7×10^{-5}
x_+			1	1.0×10^{-1}

Table 7: *Correlation matrix for $(x_\pm, y_\pm)$ cartesian coordinates, for the $D^0\pi$ decay mode.*

Observable	x_-	y_-	x_+	y_+
x_-	1	-5.1×10^{-2}	5.3×10^{-4}	-2.6×10^{-3}
y_-		1	-5.2×10^{-4}	-1.2×10^{-3}
x_+			1	1.9×10^{-2}

Table 8: *Correlation matrix for* $(x^*_\pm, y^*_\pm)$ *cartesian coordinates, for the* $D^{*0}\pi$ *decay mode.*

Parameter	1σ	1.96σ
r_B	[0.003,0.038]	[0,0.052]
γ	[-38,79] [142,259]	–
δ	[175,293] [-5,113]	–
r^*_B	[0.027],0.070]	[0.004,0.093]
γ^*	[31,92] [211,272]	[-10,144] [170,324]
δ^*	[48,108] [228,288]	[5,159] [185,339]

Table 9: *The* 1σ *(*1.96σ*) intervals for* r_B*,* δ*,* γ *(*$D^0\pi$*) and* r^*_B*,* γ^* *and* δ^* *(*$D^{*0}\pi$*). For* γ *and* δ *the* ± 180 *degree solution is also indicated.*

Parameter	1σ	1.96σ	Central value with error (1σ)
γ	[22,76] [202,256]	–	49 ± 27
r_B	[0.002,0.030]	[0,0.049]	0.016 ± 0.014
r^*_B	[0.027],0.071]	[0,0.098]	0.049 ± 0.022
δ	[178,297] [-2,116]	–	238 ± 60
δ^*	[45,103] [224,283]	–	74 ± 29

Table 10: *The* 1σ *(*1.96σ*)* $D^0\pi$*-*$D^{*0}\pi$ *combined statistical intervals for* r_B*,* $r_B{}^*$*,* δ*,* δ^**, and* γ *(angles are in degree). In the last column the central values with* 1σ *errors are also reported. For the* γ*,* δ *and* δ^* *intervals the* ± 180 *degree solution is also indicated.*

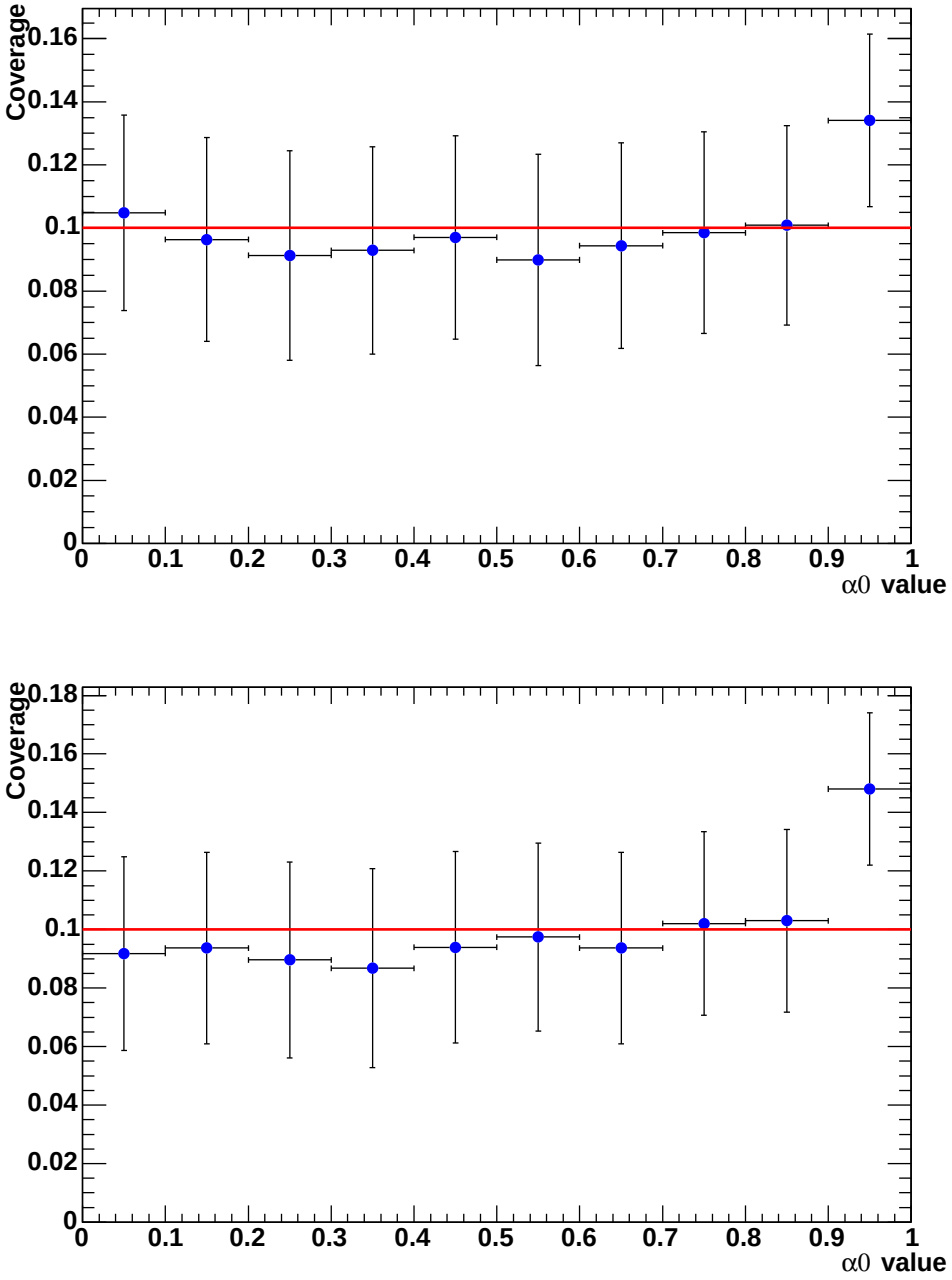

Figure 12: *Distribution of the α_0 value in the ToyMC experimental likelihood (coverage) for -1σ (top) and $+1\sigma$ (bottom) truth r_B and r_B^* values (table 5). The red lines represent the perfect coverage case, blue points are the coverage value from the ToyMC experiments for each α_0 bin of size 0.1. The error bars are due to the limited statistics of experiments (10K). Within errors, the coverage is correct for all the possible confidence level values.*

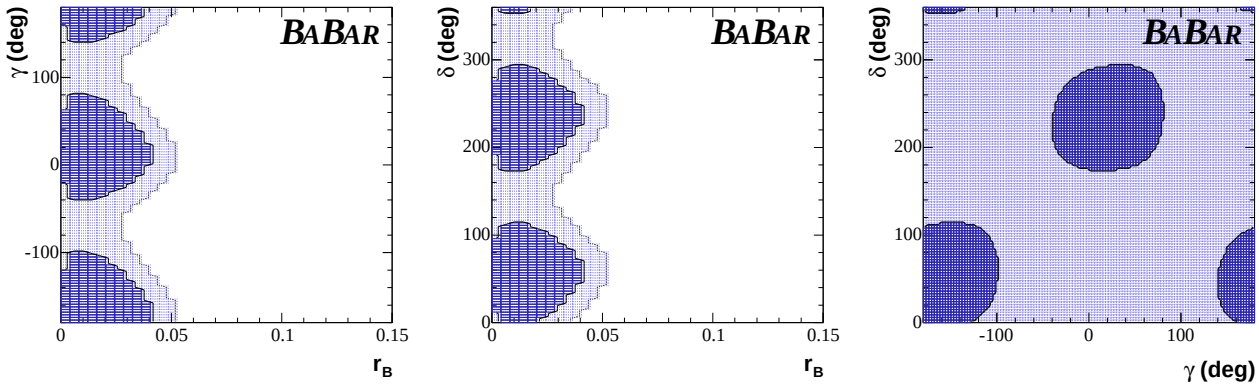

Figure 13: *2-dimensional projections of the 19.9% (dark blue) and 72.1% (bright blue) confidence-level 3-dimensional regions for the $D^0\pi$ mode.*

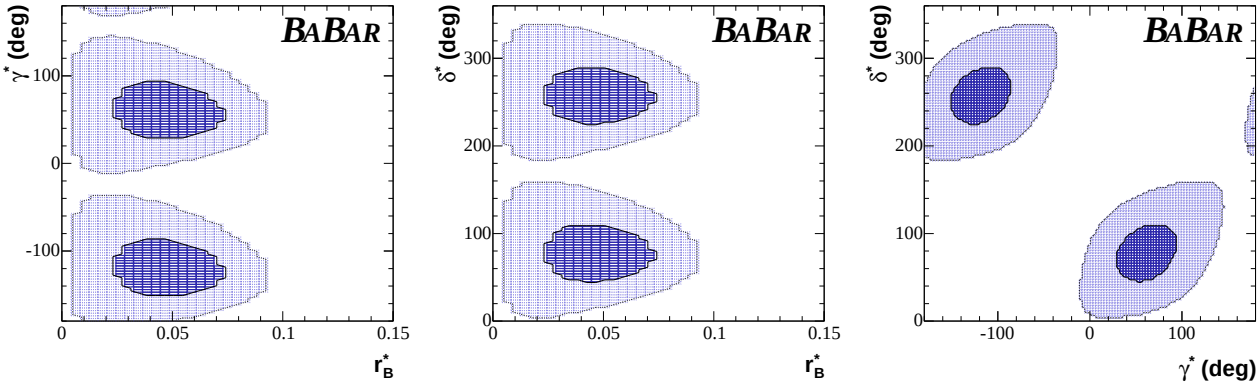

Figure 14: *2-dimensional projections of the 19.9% (dark blue) and 72.1% (bright blue) confidence-level 3-dimensional regions for the $D^{*0}\pi$ mode.*

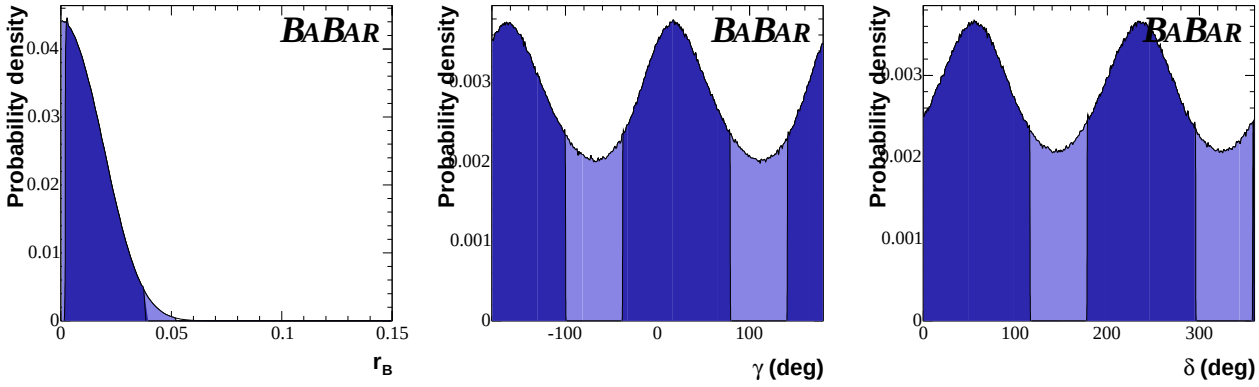

Figure 15: *Probability density functions for r_B, γ and δ together with the 1-dimensional projections of the 19.9% (dark blue) and 72.1% (bright blue) confidence-level 3-dimensional regions for the $D^0\pi$ mode.*

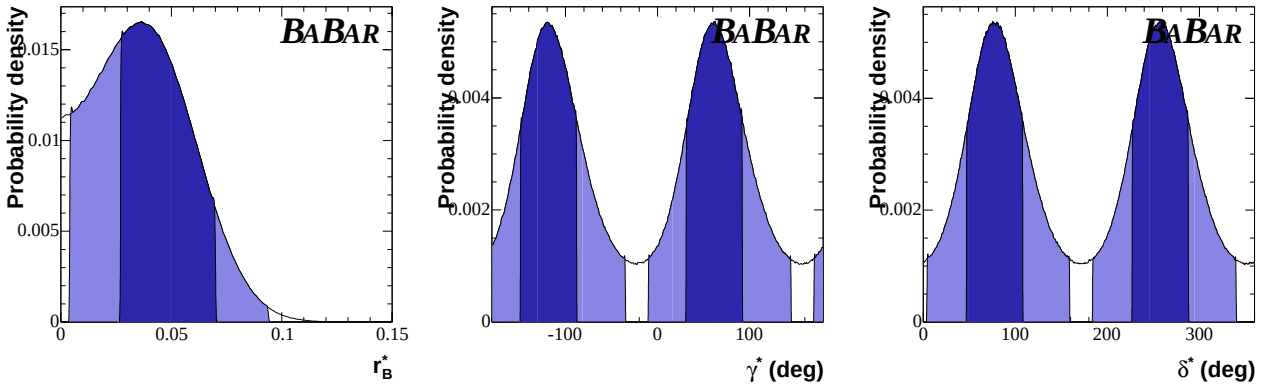

Figure 16: *Probability density functions for $r_B{}^*$, γ and δ^* together with the 1-dimensional projections of the 19.9% (dark blue) and 72.1% (bright blue) confidence-level 3-dimensional regions for the $D^{*0}\pi$ mode.*

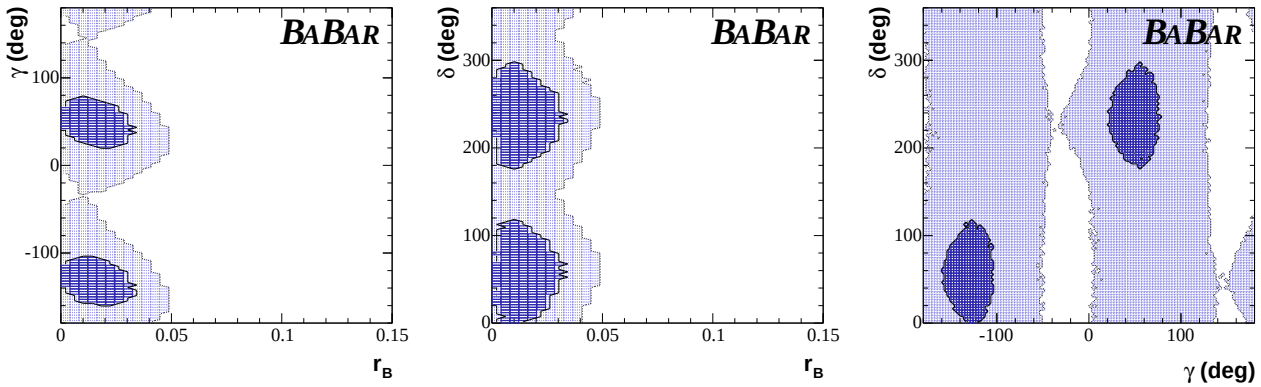

Figure 17: *2-dimensional projections of the 3.7% (dark blue) and 42.8% (bright blue) confidence-level 5-dimensional regions for the $D^0\pi$ - $D^{*0}\pi$ combined mode. The r_B and δ variables are for the $D^0\pi$ decay sample.*

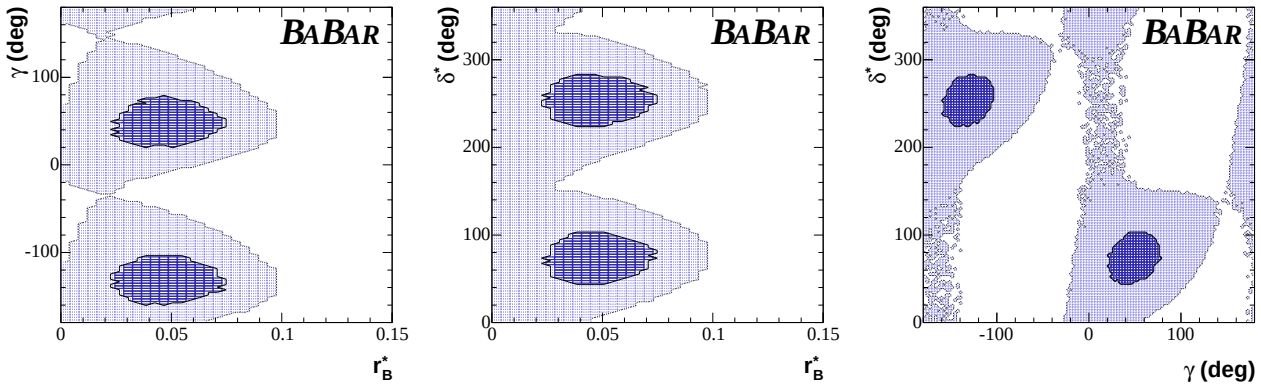

Figure 18: *2-dimensional projections of the 3.7% (dark blue) and 42.8% (bright blue) confidence-level 5-dimensional regions for the $D^0\pi$ - $D^{*0}\pi$ combined mode. The $r_B{}^*$ and δ^* variables are for the $D^{*0}\pi$ decay sample.*

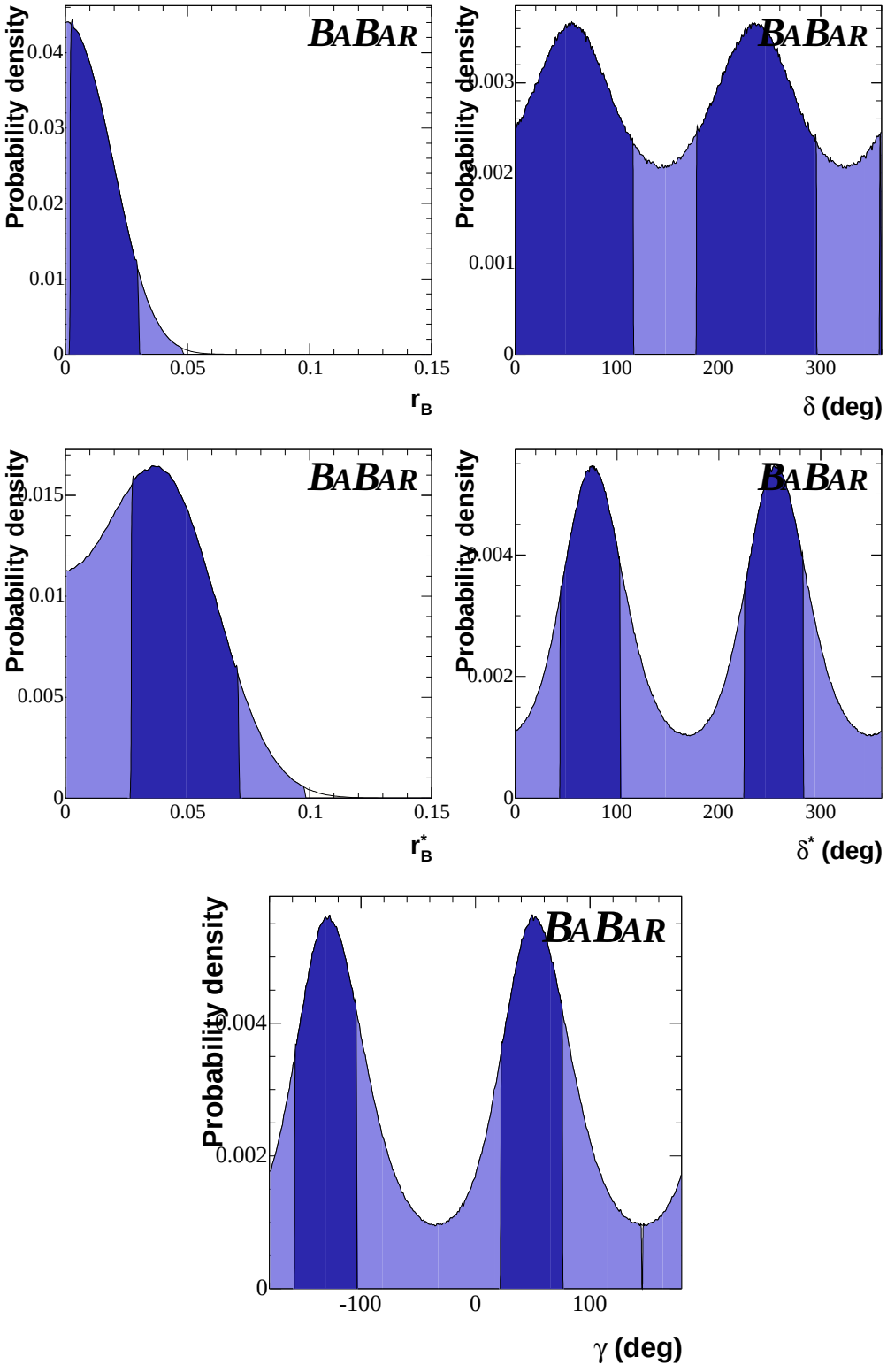

Figure 19: *Probability density functions for r_B, δ, $r_B{}^*$, δ^* and γ together with the 1-dimensional projections of the 3.7% (dark blue) and 42.8% (bright blue) confidence-level 5-dimensional regions for the $D^0\pi$ - $D^{*0}\pi$ combination.*

3 Systematic uncertainties

With the frequentist method described previously, systematic uncertainties can be included very easily just by replacing $\sigma_{x_\pm}$ and $\sigma_{y_\pm}$ by $\sqrt{\sigma^2_{x_\pm} + \sigma^2_{x_{\pm,syst}}}$ and $\sqrt{\sigma^2_{y_\pm} + \sigma^2_{x_{\pm,syst}}}$, respectively. As the statistical uncertainties dominate yet this measurement and the largest systematic uncertainties are uncorrelated among the two samples, it is appropriate to assume that the global correlations $\rho_\pm$ remain unchanged with respect to their statistical values. In any case, it has been checked that the impact of the correlation on the confidence regions/intervals is very small (this check was performed using the average correlation from Toy MC experiments instead of the values measured in the data). Table 11 summarizes the main systematic uncertainties of the measurement in cartesian coordinates, for the D^0K and $D^{*0}K$ decay modes. For comparison, we indicate the Dalitz model systematics by using the CLEO model –like the nominal one but excluding the following resonances: σ_1, σ_2, $K_0^*(1430)$ DCS, $K_2^*(1430)$ DCS, $K^*(1410)$, and $\rho(1450)$– and a model like the nominal one but excluding only the σ_1 and σ_2 resonances. We use the CLEO model to quote final Dalitz model systematics, but the alternative model excluding only the σ's has essentially the same effect, on both cartesian and polar variables; in other words, the Dalitz model effect is almost exclusively due to the non well established σ_1 and σ_2 resonances.

Table 12 reports the 1σ and 1.96σ intervals for ${r_B}^{(*)}$, γ, and $\delta^{(*)}$, as obtained by repeating the frequentist procedure with each systematic uncertainty contribution included. In the last column of the table we also report the central values with 1σ error breakdown (statistical, experimental systematic and Dalitz model systematic). Each systematic error contribution to ${r_B}^{(*)}$, γ, and $\delta^{(*)}$ is obtained by subtracting in quadrature to the statistical error (as given in table 5) the error obtained after applying the frequentist procedure using the corresponding $\sigma_{x_{\pm,syst}}$ and $\sigma_{x_{\pm,syst}}$ contribution. The central values reported are those obtained when only statistical errors are used. The asymmetry of the systematic errors is due to the change of mean values of the intervals when systematic errors are included.

The significance of *CP* violation becomes now 51.2% CL in $\mathbf{p}^{\rm t} = (r_B^t, \gamma^t, \delta^t)$=(0.038,0°,116°) for D^0K, 75.9% CL in $\mathbf{p}^{\rm t} = (r_B^{*t}, \gamma^t, \delta^{*t})$ =(0.078,0°,279°) for $D^{*0}K$, and 65.1% CL in $\mathbf{p}^{\rm t} = (r_B^t, \gamma^t, \delta^t, r_B^{*t}, \delta^{*t})$=(0.033,0°,117°,0.082,279°) for the combined measurement. These confidence levels correspond to the 1.56, 2.05, and 2.36 standard deviation ellipsoids (88.1%, 96.0%, and 98.2% probability content for the case of 1-dimensional Gaussian distributions).

In the following subsections we describe how each systematic uncertainty contribution in the cartesian coordinate space has been evaluated.

3.1 $m_{\rm ES}$, ΔE and Fisher shapes

The effect of fixing the PDF shapes in the *CP* fit has been evaluated by performing a simultaneous PDF shape and *CP* fit. Since the extraction of the shapes relies mainly on the $D\pi$ sample, the *CP* and shapes fit is performed simultaneously to the DK and $D\pi$ samples, whith shapes fixed and floated. The systematics was then taken as the quadratic difference of the errors reported by the two fits. In all cases the difference between the central values of the two fits is well below the statistical difference.

The $m_{\rm ES}$ endpoint in the Argus parameterization is fixed in the nominal fit to 5.290 GeV (the same value is also used as integration limit of the $m_{\rm ES}$ PDF). To estimate the effect of it in the determination of the signal yields and its impact on the *CP* parameters we have varied it by ± 0.5 MeV. It was found to be completely negligible.

Source	x_+	y_+	x_-	y_-	x_+^*	y_+^*	x_-^*	y_-^*
$m_{\rm ES}, \Delta E, \mathcal{F}$ shapes	0.0105	0.0086	0.0088	0.0141	0.0196	0.0218	0.0218	0.0146
Real D^0 fraction	0.0050	0.0047	0.0061	0.0036	0.0035	0.0049	0.0028	0.0032
Right sign D^0's	0.0157	0.0090	0.0070	0.0211	0.0065	0.0163	0.0108	0.0103
Eff. in the Dalitz plot	0.0078	0.0085	0.0089	0.0119	0.0067	0.0119	0.0040	0.0079
Tracking efficiency	0.0082	0.0080	0.0095	0.0123	0.0058	0.0109	0.0051	0.0046
Cont bkg. Dalitz shape	0.0195	0.0096	0.0160	0.0149	0.0133	0.0084	0.0083	0.0046
BB bkg. Dalitz shape	0.0026	0.0072	0.0069	0.0130	0.0061	0.0098	0.0029	0.0003
Invariant mass resolution	0.0031	0.0023	0.0022	0.0016	0.0031	0.0023	0.0022	0.0016
Dalitz amplitude and phases	0.0012	0.0069	0.0050	0.0033	0.0043	0.0138	0.0079	0.0079
SubTotal	0.0301	0.0226	0.0258	0.0368	0.0275	0.0373	0.0280	0.0223
Dalitz model (CLEO)	0.0324	0.0214	0.0185	0.0424	0.0253	0.0560	0.0206	0.0249
Total (CLEO)	0.0442	0.0311	0.0318	0.0561	0.0374	0.0673	0.0348	0.0334
Dalitz model (no σ_1, σ_2)	0.0336	0.0258	0.0207	0.0374	0.0255	0.0464	0.0209	0.0396
Total (no σ_1, σ_2)	0.0451	0.0343	0.0331	0.0525	0.0375	0.0595	0.0349	0.0454

Table 11: *Summary of the contributions to the systematic error in cartesian coordinates,* $(x_\pm, y_\pm)$ *and* $(x_\pm^*, y_\pm^*)$.

Parameter	1σ	1.96σ	Central value with error (1σ)
γ	[36,106] [216,286]	[13,136] [193,316]	$70 \pm 31 \,^{+12}_{-10}\,^{+14}_{-11}$
r_B	[0.025,0.211]	[0,0.277]	$0.118 \pm 0.079 \pm 0.034 \,^{+0.036}_{-0.034}$
r_B^*	[0.066],0.274]	[0,0.352]	$0.169 \pm 0.096 \,^{+0.030}_{-0.028}\,^{+0.029}_{-0.026}$
δ	[48,155] [228,335]	–	$104 \pm 45 \,^{+17}_{-21}\,^{+16}_{-24}$
δ^*	[251,342] [71,162]	–	$296 \pm 41 \,^{+14}_{-12} \pm 15$

Table 12: *The* 1σ *(*1.96σ*)* D^0K*-*$D^{*0}K$ *combined intervals including systematic uncertainties for* r_B*,* $r_B{}^*$*,* δ*,* δ^* *and* γ *(angles are in degree). In the last column the central values with* 1σ *error break-down are reported: the first errors are statistical, the second are experimental systematics, and the third are Dalitz model systematics. For the* γ*,* δ *and* δ^* *intervals the* ± 180 *degree solution is also reported.*

3.2 Background composition

The uncertainty due to the fraction of real D^0's in background (table 38 of Ref. [2]) is estimated by varying this parameter within its statistical error and then repeating the fit to the data sample. In order to be conservative, we have moved up and down by one sigma these fractions for all the samples –D^0K, $(D^0\pi^0)K$ and $(D^0\gamma)K$– and components (Cont and $B\overline{B}$) simultaneously. In the case of the $B\overline{B}$ fraction for D^0K events, an upper limit of 10% was used to evaluate this systematics. The larger between the half difference between the two fits and the quadratic difference of the fit errors is assigned as systematic uncertainty.

A potential difference in the number of real D^0's in the continuum background between B^+ and B^- events could fake *CP* violating effects in the signal. No significant difference between B^+ and B^- has been found in MC. Nevertheless, we account for any potential effect by introducing an independent set of *CP* parameters for the continuum background with a real D^0. By repeating the nominal fit with this new set of parameters we found a negligible impact on the *CP* parameters.

The fraction of right sign (RS) D^0's is taken from MC simulation. We have estimated this contribution from the variation of the *CP* parameters in the fit to the data sample when a value of 0.5 is assumed instead of the nominal values (given in table 38 of Ref. [2]). As before, we take the larger between the difference of central values and the quadratic difference of fit errors. The change observed on the *CP* parameters is consistent with the larger between the bias and the rms from a set of Toy MC experiments generated with the nominal value and fit with 0.5.

3.3 Dalitz efficiency

To estimate the effect from the Dalitz efficiency the nominal *CP* fit was repeated by assuming a flat distribution instead of the nominal 3rd order polynomial parameterization (table 38 of Ref. [2]). In addition, we have evaluated a systematics due to tracking and K^0_S reconstruction efficiency over the Dalitz plot. It has been evaluated by repeating the fit using alternative values of the 3rd order polynomial parameterization coefficients with: i) the tracking efficiency correction applied on the 2 pions from the D^0 decay and the bachelor kaon (table 10 of Ref. [2]); and ii) tracking efficiency correction applied to the pions from the K^0_S decay (table 11 of Ref. [2]). In all cases, we take the larger between the difference of central values and the quadratic difference of fit errors. The uncertainties from the two corrections have been added quadratically.

3.4 Dalitz shape for combinatorial background

The Dalitz shape for combinatorial continuum events is estimated by using off-resonance data, as described in sections 3 and 5 of Ref. [2]. The correction for $B\overline{B}$ combinatorial background is obtained from Monte Carlo simulation. The systematics from this correction is estimated from the difference on the *CP* parameters when flat distributions are assumed instead. We take the larger between the difference of central values and the quadratic difference of fit errors.

3.5 Limited mass resolution

The nominal Dalitz model assumes perfect mass resolution. Given that all the resonances present in the $D^0 \to K^0_S\pi^+\pi^-$ decay are quite wide compared to the estimated mass resolution (about 4 MeV^2 for a $K^0_S\pi^+$ mass squared of about 1 GeV^2 [6]), we expect the effect to be completely negligible. Only the $\omega(782)$ has an intrinsic width comparable to the mass resolution (about 6 MeV^2 for a squared $\pi^+\pi^-$ mass of 0.8 GeV^2 [6]), but the sensitivity of the *CP* parameters is in this case suppressed. To evaluate the effect of the limited mass resolution on the Dalitz plot, two

different fits were performed to the reweighted signal MC (see section 10.3 of Ref. [2]). The first fit used the reconstructed $K^0_S\pi^+$ and $K^0_S\pi^-$ masses, while the second was performed with the MC truth masses (perfect resolution). The difference of fit values was taken as our systematic uncertainty. The errors from the fit for the different parameters were basically unchanged between the two fits.

3.6 Dalitz PDF normalization

We have investigated a possible systematic uncertainty due to the limited numerical precision in the evaluation of the Dalitz plot PDF normalization integral. It has been done by increasing by a factor 25 the number of cells in the integration grid, on both Toy MC experiments and the data fit. This corresponds to 5 times more bins on each dimension, i.e. $N_{grid} = 200 \rightarrow 1000$, or equivalently a precision of 1.1 MeV precision on the $K^0_S\pi^+$ and $K^0_S\pi^-$ masses. In both cases the change in the *CP* parameters was found to be negligible. As cross-check, the nominal fit was also redone by using Vegas Monte Carlo integration with $N_{Vegas} = 1.6 \times 10^7$ events. Again, the effect on the *CP* parameters was found equally to be negligible.

3.7 Statistical errors on Dalitz amplitudes and phases

The phases and amplitudes of the Dalitz model are fixed to the values found from the fit to the high statistics $D^{*+} \rightarrow D^0\pi^+_s$ sample. We expect its effect to be negligible. Nevertheless, we estimated its effect by performing a simultaneous DK and $D^{*+} \rightarrow D^0\pi^+_s$ fit with all these parameters floated. The uncertainty is taken as the larger between the difference of central values and the quadratic difference of the errors reported by the two fits. The difference of central values is in all cases consistent with the quadratic difference of the statistical errors.

3.8 Dalitz model systematics

The Dalitz model systematics is the single most important contribution to the total systematic uncertainty. To evaluate it, we generated about 500 Toy Monte Carlo experiments (signal Dalitz only) tunned to the data sample using the nominal Dalitz model. The experiments were then fit using the nominal model, the CLEO model (the nominal model but excluding the σ_1, σ_2, $K^*_0(1430)$ DCS, $K^*_2(1430)$ DCS, $K^*(1410)$, and $\rho(1450)$ resonances), and a third model identical to the nominal one but excluding only the σ_1 and σ_2 resonances. To get ride of statistical fluctuations and avoid double counting with the data statistical error, each sample was generated with *infinite* statistics (in practice, 10K events per B decay channel). To be conservative, only D^0K and $(D^0\pi^0)K$ events have been used (10K events each) since it was found that the effect for $(D^0\pi^0)K$ and $(D^0\gamma)K$ is anticorrelated due to the effective π radians shift between the strong phases, which change the sign for all cartesian components (sine and cosine terms). The systematic uncertainty is finally assigned as the quadratic sum of the mean and rms of the experiment-by-experiment differences.

The problem with this technique is which values for r^t_B, r^{*t}_B, γ^t, δ^t, and δ^{*t} are used in the generation of the experiments. Given the current large statistical errors (table 5), taking the central values would be just a choice among others, especially if the effect turns out to be multiplicative with the truth (generated) value. Unfortunately, it has been verified that the systematic uncertainty for all cartesian components evaluated in this way strongly depends with the values of r^t_B and r^{*t}_B (increases almost linearly with it, since cartesian *CP* parameters depend linearly with r_B and r^*_B), and smoothly with the values of γ^t, δ^t, and δ^{*t}. This dependency has also been verified when the *CP* fit is performed to ${r_B}^{(*)}$, γ and $\delta^{(*)}$ directly. For example, for $r^t_B = 0.12$ the effect on γ is about 10°, but for $r^t_B = 0.03$ it is about 14°. On the contrary, the change on $r_B(r^*_B)$ itself increases almost linearly with $r^t_B(r^{*t}_B)$. These dependencies have also been noticed by Belle [4], and the solution they

have adopted and claimed to be conservative is to scan the phases for fixed $r_B^t = 0.13$, taking the largest variation from the scan. However, we do not agree with this solution since fixing $r_B^t = 0.13$ does not seem to be conservative enough.

The solution we have finally adopted to quote the Dalitz model systematics is the following. As we know that cartesian coordinates behave almost perfectly as independent Gaussians, for each single experiment we generate randomly all the 8 cartesian components, following independent Gaussian distributions with mean and width values as measured in the data (table 3). The rest of the procedure is identical to what was described above. Taking the systematic uncertainty from the mean and rms of the experiment-by-experiment differences for each component, we integrate over the others, which is exactly what we want (meaning of 1σ interval, independent of all the other variables). Note that this procedure cannot be used in polar coordinates due to the non-Gaussian behavior in this case, in addition to the large correlation among these parameters. The distributions of the experiment-by-experiment differences are shown in figures 20 and 21, for the CLEO and no σ's models, respectively. The quadratic sum of the offsets and rms' are quoted in table 11.

All the three Dalitz models used are based on Breit-Wigner parameterization of resonances, except for the $\rho(770)$ and $\rho(1450)$ for which we use Gounaris-Sakurai parametrization to model better the tails. Since Breit-Wigner amplitudes can only describe well narrow resonances, we introduced the Blatt-Weisskopf penetration factors for the intermediate resonances and a resonance width q^2 dependence to deal with broad states. These quantities and models have, however, large theoretical uncertainties and might be a substantial source of systematic uncertainties. To evaluate these potential effects we have also used two alternative Dalitz models, one using Breit-Wigners also for the $\rho(770)$ and $\rho(1450)$ resonances, and the other without Blatt-Weisskopf form factors. Figures 22 and 23 show the experiment-by-experiment differences for these two models. The mean and rms values are found to be completely negligible.

As a final check related to the Dalitz model we have studied the impact on the *CP* parameters by imposing the constraint that the phase difference between doubly-Cabibbo suppressed (DCS) and Cabibbo favored (CF) K^* resonances below 1.440 GeV/c^2 ($K\eta'$ threshold) is $(-1)^J$. This is a consequence of the Watson theorem [7]. The constraint applies to $K^*(892)$, $K_0^*(1430)$ and $K_2^*(1430)$, which should have a DCS-CF relative phase of 180°, 0° and 0°, respectively. An inspection to tables 30 and 31 of Ref. [2] reveals that the fit results to the D^* sample are consistent with this prediction, within statistical errors. To perform this check we have repeated the D^* Dalitz fit imposing the constraint on the DCS-CF relative phases, and then the *CP* parameters were obtained by repeating the *CP* fit with this constraint applied. Table 13 shows the *CP* fit results obtained with this constraint. These results should be compared to those of table 3. The results of both fits are consistent within the statistical differences, while there is no evidence of improvement in statistical power. Therefore, no systematic error is assigned. The same conclusion is obtained when the fit is performed in polar coordinates.

Observable	D^0K	$D^{*0}K$
x_-	0.0776 ± 0.0689	-0.1325 ± 0.0934
y_-	0.0613 ± 0.0926	-0.1401 ± 0.1061
x_+	-0.1258 ± 0.0703	0.1333 ± 0.0925
y_+	0.0081 ± 0.0792	0.0213 ± 0.1226

Table 13: *Fit results for $(x_\pm, y_\pm)$ cartesian coordinates with the constraint $(-1)^J$ on the phase difference between doubly-Cabibbo suppressed (DCS) and Cabibbo favored (CF) $K^*(892)$, $K_0^*(1430)$ and $K_2^*(1430)$ resonances applied, for the D^0K and $D^{*0}K$ decay modes.*

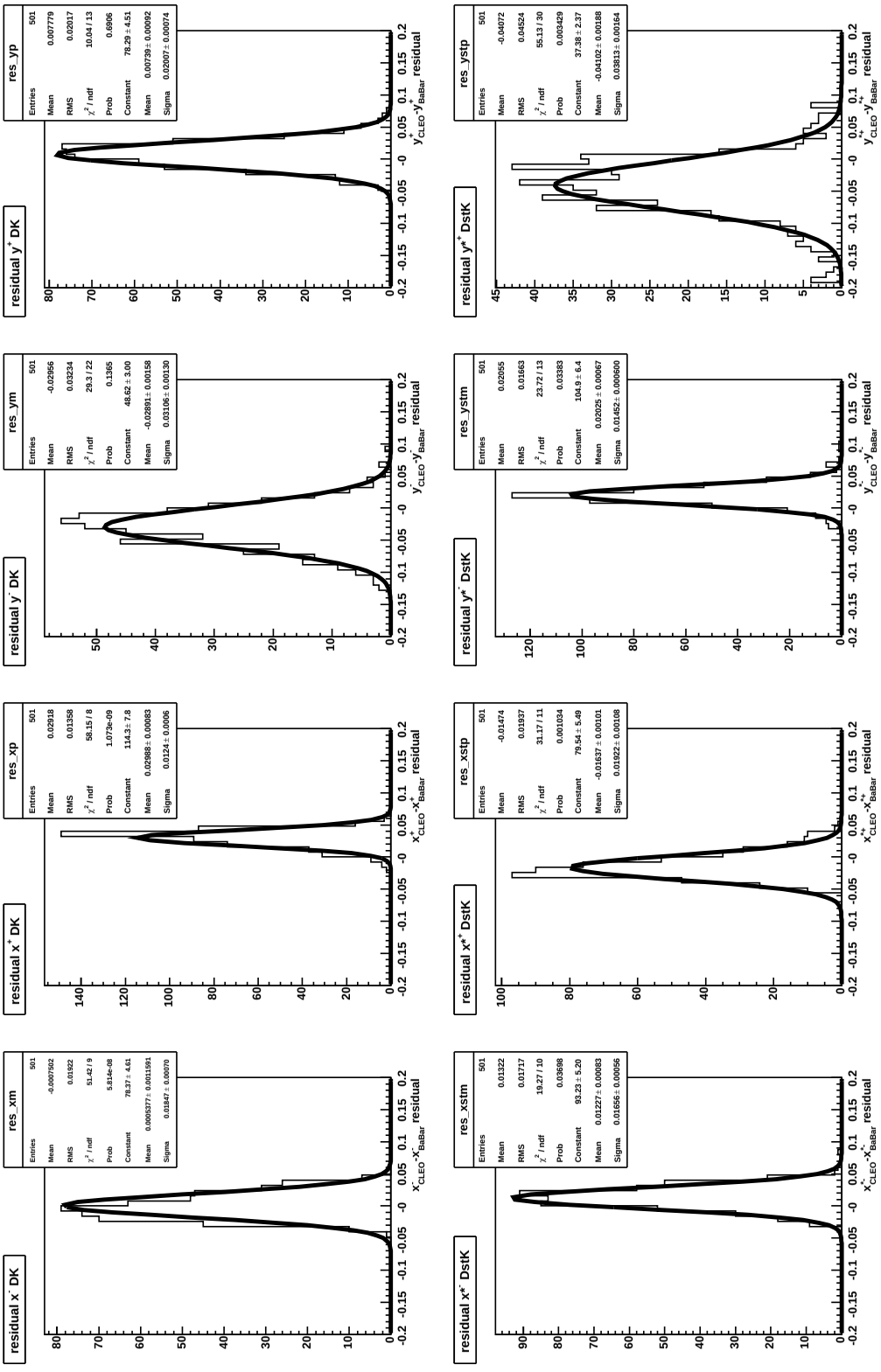

Figure 20: *Experiment-by-experiment differences of the cartesian CP fit parameters using the reference and the CLEO Dalitz models. The systematic error for each component is quoted as quadratic sum of the bias and the rms.*

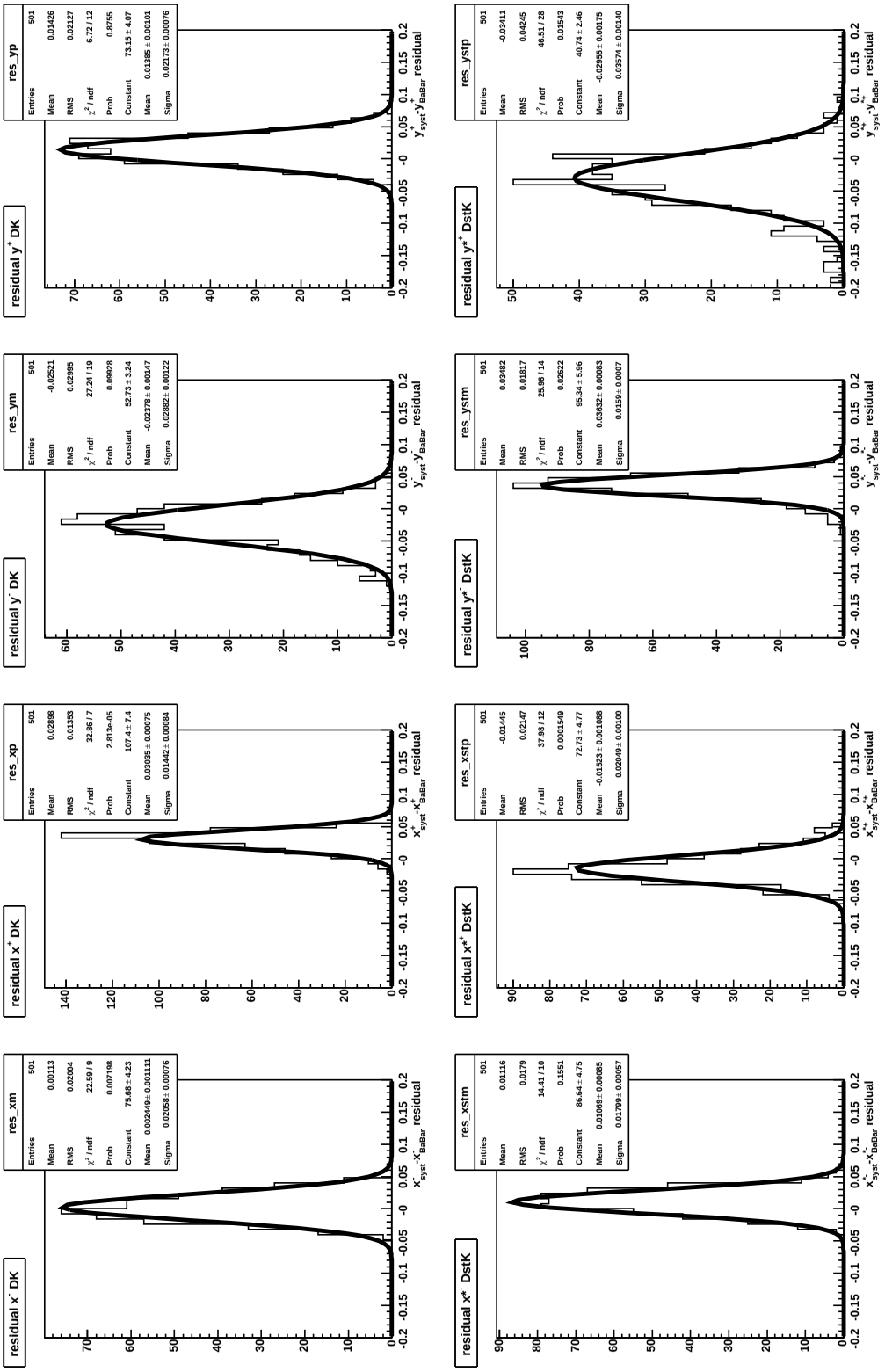

Figure 21: *Experiment-by-experiment differences of the cartesian CP fit parameters using the reference Dalitz model and the same model without the σ_1 and σ_2 resonances. The systematic error for each component is quoted as quadratic sum of the bias and the rms.*

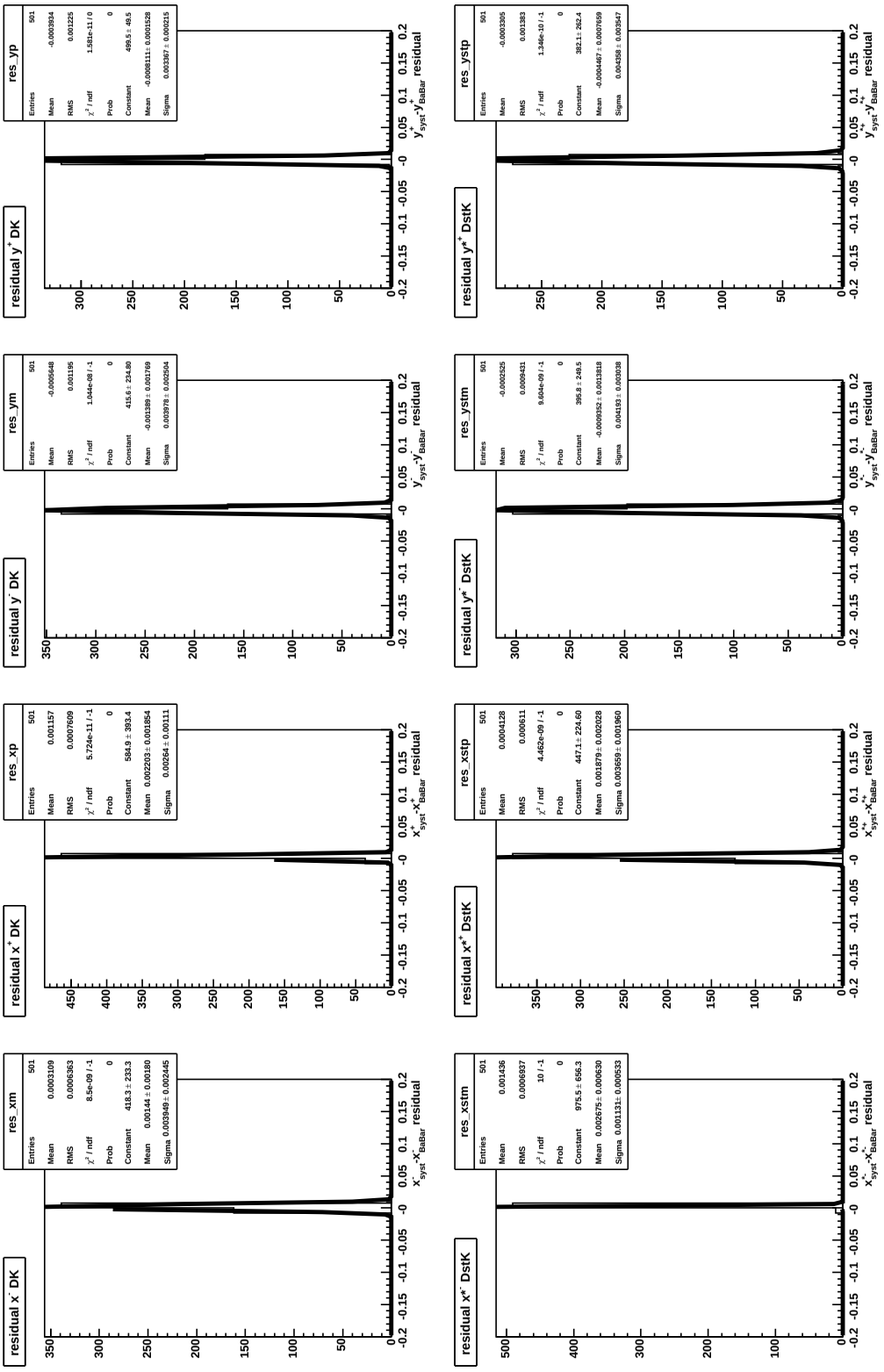

Figure 22: *Experiment-by-experiment differences of the cartesian CP fit parameters using the reference Dalitz model and the same model with all Breit-Wigners.*

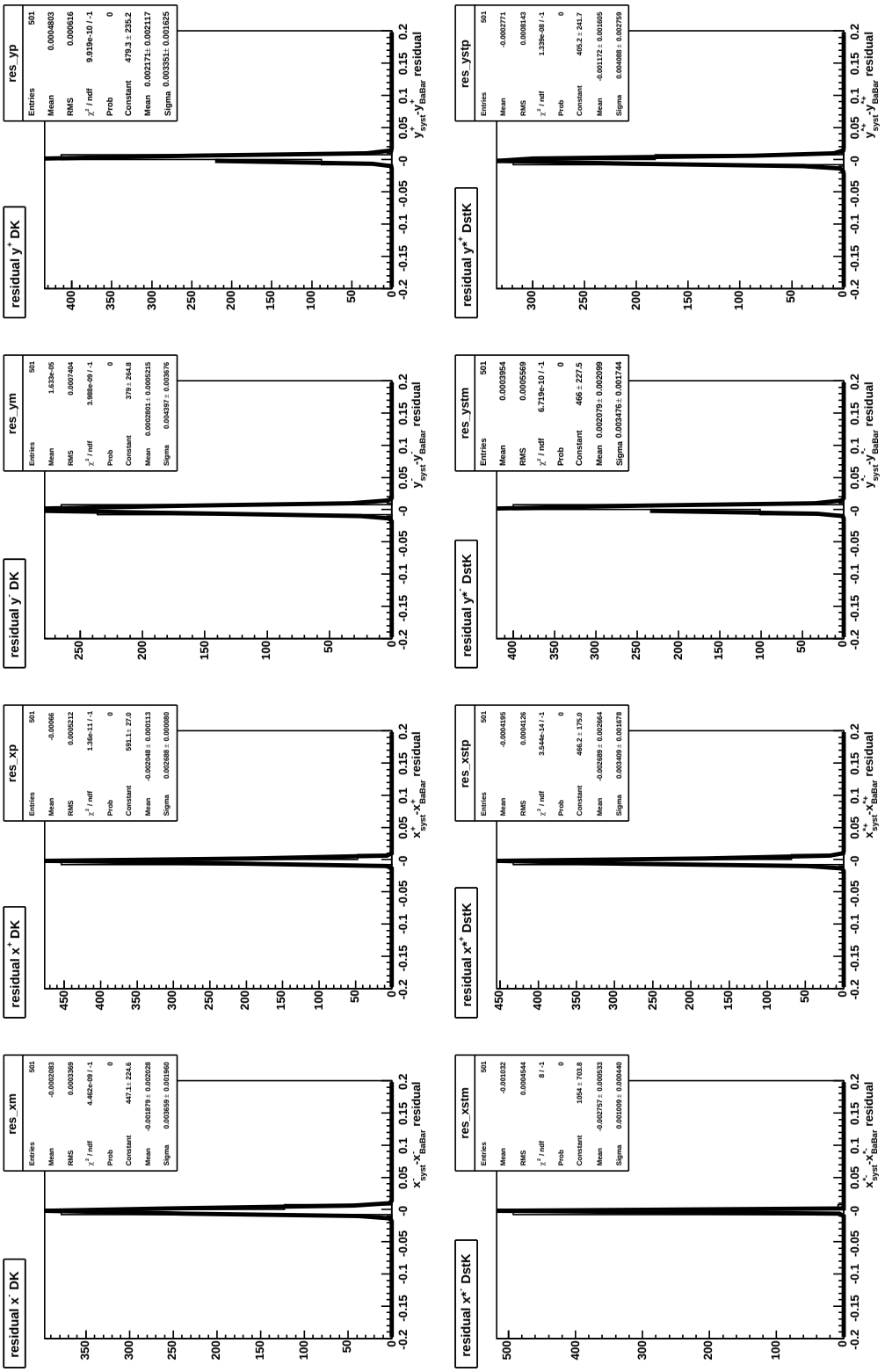

Figure 23: *Experiment-by-experiment differences of the cartesian CP fit parameters using the reference Dalitz model and the same model without Blatt-Weisskopf form factors.*

4 Bayesian technique

4.1 Description of the method

The estimation of the confidence regions/intervals with the Bayesian approach requires the evaluation of the likelihood function $\mathcal{L}_{exp} \equiv \mathcal{L}_{exp}(r_B, \gamma, \delta)$ in the whole range of definition of r_B, γ and δ, $[0, 1]$, [-π,π] and [0,2π], respectively, with the yields floated at each given *CP* point. The estimate of the confidence region for the *CP* parameters implies a choice of a priori distribution. For this check we arbitrarily assume a uniform a priori distribution for each of the *CP* parameters r_B, γ and δ.

We define confidence region $D(\mathcal{C})$ at a given $\mathcal{C}$ confidence level the region in γ-r_B space such

$$\frac{\int_{D(\mathcal{C})} dr_B d\gamma \int_0^{2\pi} d\delta \mathcal{L}_{exp}(r_B, \gamma, \delta)}{\int_0^1 \int_{-\pi}^{\pi} \int_0^{2\pi} \mathcal{L}_{exp}(r_B, \gamma, \delta)\, dr_B d\gamma d\delta} = \mathcal{C} \ . \tag{15}$$

The $D(\mathcal{C})$ definition is arbitrary (this is always the case for confidence region) and we choose to define it by starting the integration procedure by the maximum of the likelihood function and by requiring that the likelihood value at any point in the boundary of D be the same (integration over all likelihood values larger than the value at the boundary). Notice that this can easily give disjoint region.

Similarly we can define the 1-dimensional confidence interval at $\mathcal{C}$ confidence level for, say, r_B, as

$$\frac{\int_{I(C)} dr_B \int_{-\pi}^{+\pi} d\gamma \int_0^{2\pi} d\delta \mathcal{L}_{exp}(r_B, \gamma, \delta)}{\int_0^1 \int_{-\pi}^{\pi} \int_0^{2\pi} \mathcal{L}_{exp}(r_B, \gamma, \delta)\, dr_B d\gamma d\delta} = \mathcal{C} \ , \tag{16}$$

where again $I(\mathcal{C})$ can be a set of disjoint interval.

In this way we expect that such intervals have the correct coverage. Notice that the effect of the bias on r_B is completely irrelevant for γ and δ measurements (we make no use of the concept of fitted r_B value).

4.2 1- and 2-dimensional confidence regions for D^0K and $D^{*0}K$

In figure 24 we show the confidence region for $\gamma^{(*)}$ versus ${r_B}^{(*)}$, for D^0K and $D^{*0}K$. The red region is the 68% CL region while the yellow one is the 95% CL. Similarly, figures 25 and 26 show the confidence regions for $\gamma^{(*)}$ versus $\delta^{(*)}$ and $\delta^{(*)}$ versus ${r_B}^{(*)}$, for D^0K and $D^{*0}K$. In figures 27 and 28 we show the probability density functions for ${r_B}^{(*)}$, $\gamma^{(*)}$ and $\delta^{(*)}$ for D^0K and $D^{*0}K$, respectively, obtained by integrating the experimental likelihood for all the values of the other variables: $\gamma^{(*)}$, $\delta^{(*)}$; ${r_B}^{(*)}$, $\delta^{(*)}$; and ${r_B}^{(*)}$, $\gamma^{(*)}$. On the same figures we show the confidence intervals at 68% (red) and 95% (yellow) CL. Notice that the likelihood distribution is nicely showing the $\pm\pi$ ambiguity in $\gamma^{(*)}$ and $\delta^{(*)}$. The probability density function for ${r_B}^{(*)}$ shows clearly the non-Gaussian behavior we expect from Toy MC, showing the poor sensitivity to small values of ${r_B}^{(*)}$. In figure 29 we show the probability density function for γ from the combination of the D^0K and $D^{*0}K$ likelihoods, integrated over r_B, ${r_B}^*$, δ and δ^*.

Table 14 reports the confidence intervals for the various parameters (statistical only). For the central values we quote the expectation value using the experimental likelihood, and the 1σ error is given by the 68% confidence limit region around the expectation value. For the phases we have symmetrized the errors taking the largest between the positive and negative errors. The results include the intrinsic two fold ambiguity for the weak and strong phases.

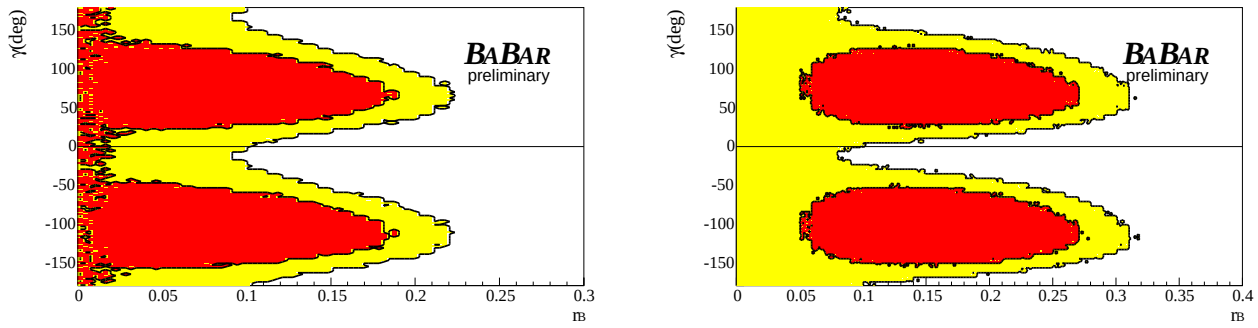

Figure 24: *68% (red) and 95% (yellow) Bayesian confidence region in $\gamma^{(*)}$-$r_B{}^{(*)}$ plane for D^0K (left) and $D^{*0}K$ (right).*

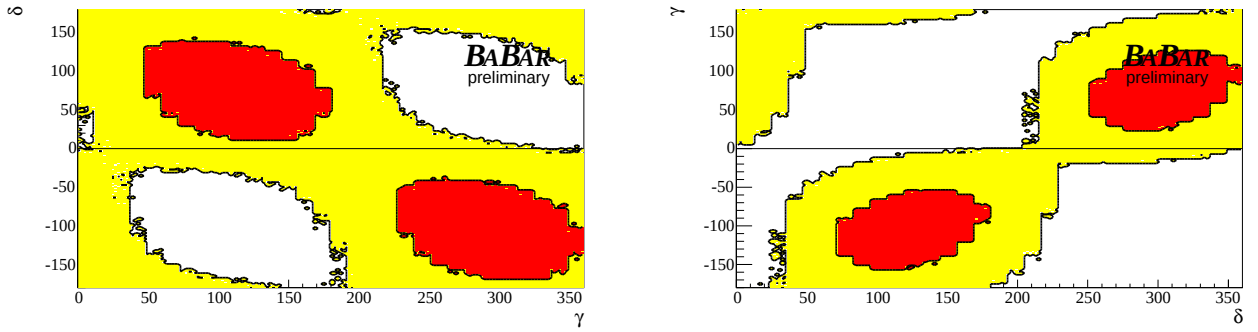

Figure 25: *68% (red) and 95% (yellow) Bayesian confidence region in $\gamma^{(*)}$-$\delta^{(*)}$ plane for D^0K (left) and $D^{*0}K$ (right).*

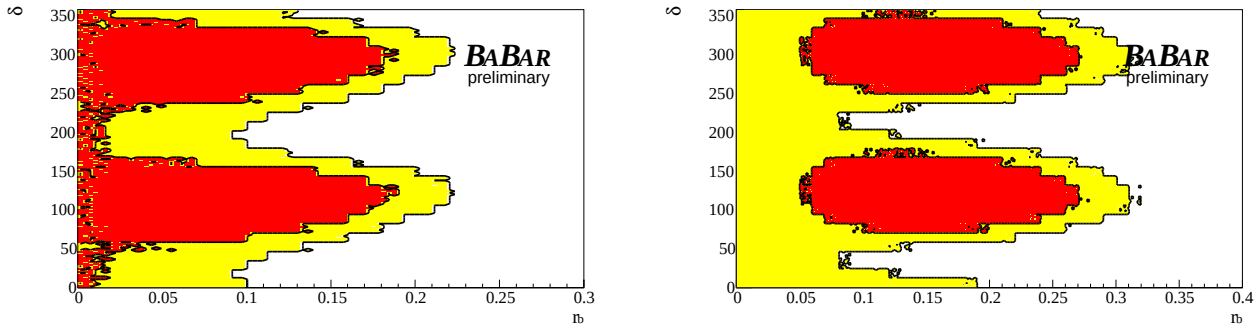

Figure 26: *68% (red) and 95% (yellow) Bayesian confidence region in $\delta^{(*)}$-$r_B{}^{(*)}$ plane for D^0K (left) and $D^{*0}K$ (right).*

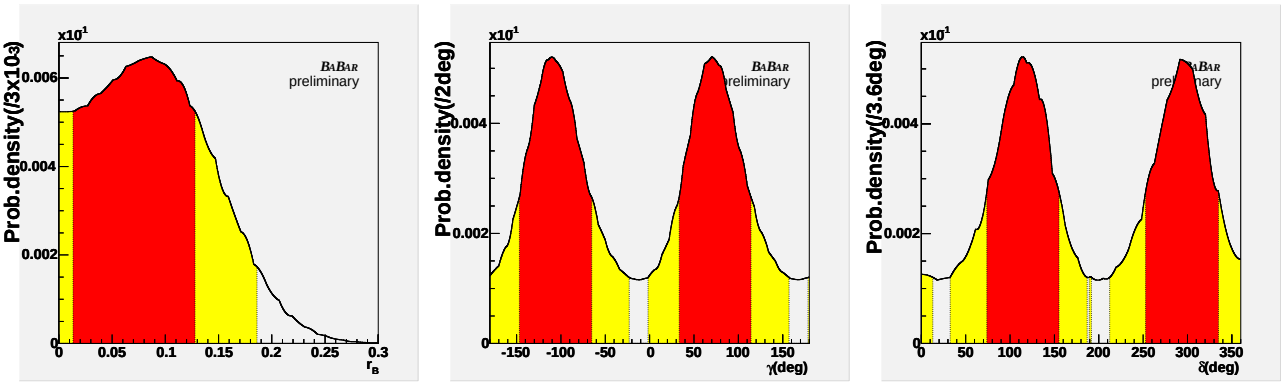

Figure 27: *Probability density functions for r_B, γ and δ for D^0K. 68% (red) and 95% (yellow) Bayesian confidence intervals are shown.*

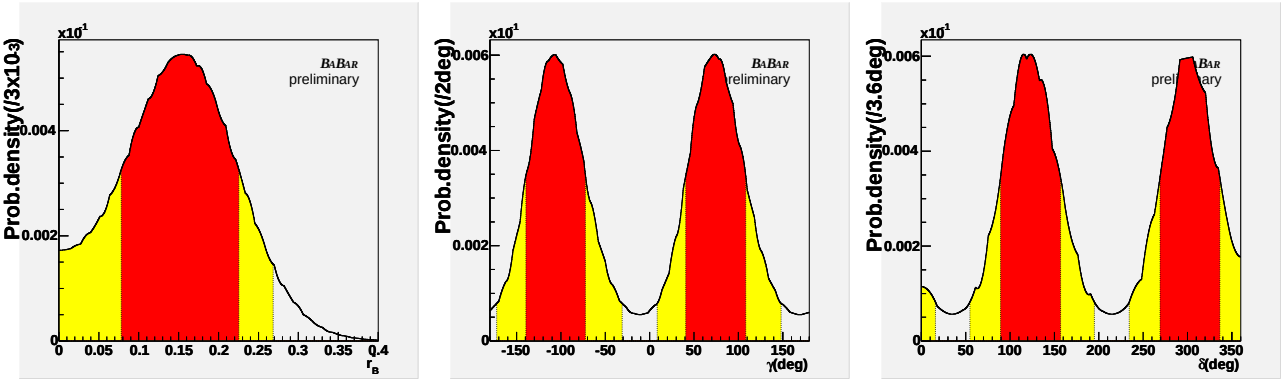

Figure 28: *Probability density functions for $r_B{}^*$, γ^* and δ^* for $D^{*0}K$. 68% (red) and 95% (yellow) Bayesian confidence intervals are shown.*

Since the frequentist method is the one adopted to quote final results no dedicated evaluation of systematic uncertainties has been performed. However, with a very good approximation we can assign the symmetrized experimental and Dalitz model systematic errors obtained in the frequentist approach, as given in table 15.

Comparing the Bayesian results with those of the frequentist method, we observe that there is a satisfactory agreement between the two methods, although the Bayesian errors tend to be smaller than those of the frequentist approach.

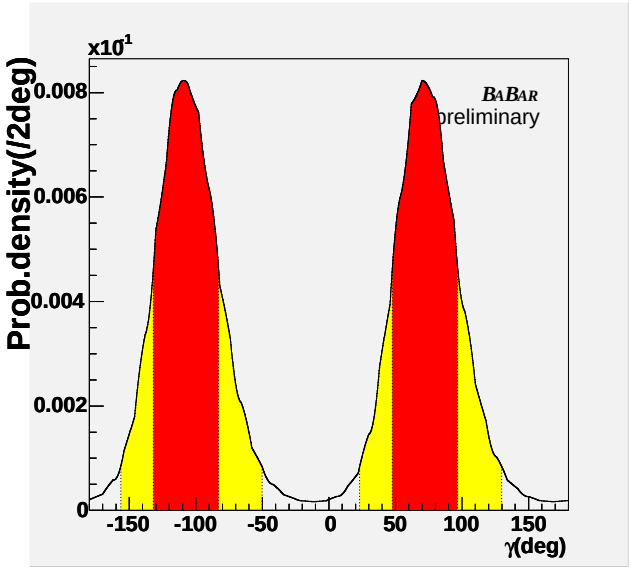

Figure 29: *Probability density function for γ for the D^0K-$D^{*0}K$ combination. 68% (red) and 95% (yellow) Bayesian confidence intervals are shown.*

Parameter	68% CL (stat. only)	95% CL (stat. only)	Central value with error (1σ)
γ	[-147,-65] [33,114]	[-180,-23] [-2,157] [179,180]	70 ± 44
γ^*	[-140,-72] [41,108]	[-172,-31] [9,148]	73 ± 35
δ	[74,155] [253,335]	[0,13] [189,192] [212,360]	114 ± 41
δ^*	[89,157] [269,337]	[0,16] [55,195] [234,360]	303 ± 34
r_B	[0.01,0.13]	[0,0.19]	$0.087^{+0.041}_{-0.074}$ $[0.071 \pm 0.058]$
r_B^*	[0.08,0.22]	[0,0.27]	$0.155^{+0.070}_{-0.077}$ $[0.152 \pm 0.074]$
γ (combined)	[-132,-83] [48,97]	[-156,-50] [23,130]	70 ± 26

Table 14: *Bayesian confidence intervals for $\gamma^{(*)}$, $\delta^{(*)}$ and $r_B{}^{(*)}$ (statistical only). Angles are given in degree. The Bayesian confidence intervals for the combination of the D^0K and $D^{*0}K$ channels is also given. In the last column the central values with 1σ errors are also reported. For the $\gamma^{(*)}$ and $\delta^{(*)}$ intervals the $\pm 180^\circ$ solution is also indicated. For the central values we quote the expectation value using the experimental likelihood, and the 1σ error is given by the 68% confidence limit region around the expectation value. For the phases we have symmetrized the errors taking the largest between the positive and negative errors.*

Parameter	Central value with error (1σ)
γ (combined)	$70 \pm 26 \pm 11 \pm 13$
δ	$114 \pm 41 \pm 19 \pm 20$
δ^*	$303 \pm 34 \pm 13 \pm 15$
r_B	$0.087^{+0.041}_{-0.074} \pm 0.034 \pm 35$ $[0.071 \pm 0.058 \pm 0.034 \pm 35]$
r_B^*	$0.155^{+0.070}_{-0.077} \pm 0.029 \pm 0.028$ $[0.152 \pm 0.074 \pm 0.029 \pm 0.028]$

Table 15: *Bayesian central values with 1σ statistical and systematic errors for γ, $\delta^{(*)}$ and ${r_B}^{(*)}$ (angles are in degree). The first errors are statistical, the second are experimental systematics and the third are Dalitz model systematics. The statistical errors are the same as those reported in table 15. The systematic uncertainties are the symmetrized systematic errors obtained with the frequentist approach, as reported in table 12.*

5 Final results

Using an integrated luminosity of 205 fb^{-1}, corresponding to the Run1-2-3-4(BlackDiamond) data sample, we have performed a Dalitz plot analysis of $B^- \to D^{(*)0}K^-$, with $D^* \to D^0\pi^0, D^0\gamma$, $D^0 \to K_S\pi^+\pi^-$ decays, obtaining the following *CP*-violating parameter results:

$$
\begin{aligned}
x_- \equiv \Re(r_{B-}e^{i\theta_-}) &= 0.077 \pm 0.069(\text{stat.}) \pm 0.026(\text{exp. syst.}) \pm 0.019(\text{model syst.}) \ , \\
y_- \equiv \Im(r_{B-}e^{i\theta_-}) &= 0.064 \pm 0.092(\text{stat.}) \pm 0.037(\text{exp. syst.}) \pm 0.042(\text{model syst.}) \ , \\
x_+ \equiv \Re(r_{B+}e^{i\theta_+}) &= -0.129 \pm 0.070(\text{stat.}) \pm 0.030(\text{exp. syst.}) \pm 0.032(\text{model syst.}) \ , \\
y_+ \equiv \Im(r_{B+}e^{i\theta_+}) &= 0.019 \pm 0.079(\text{stat.}) \pm 0.023(\text{exp. syst.}) \pm 0.021(\text{model syst.}) \ , \\
x_-^* \equiv \Re(r_{B-}^*e^{i\theta_-^*}) &= -0.131 \pm 0.093(\text{stat.}) \pm 0.028(\text{exp. syst.}) \pm 0.021(\text{model syst.}) \ , \\
y_-^* \equiv \Im(r_{B-}^*e^{i\theta_-^*}) &= -0.143 \pm 0.105(\text{stat.}) \pm 0.022(\text{exp. syst.}) \pm 0.025(\text{model syst.}) \ , \\
x_+^* \equiv \Re(r_{B+}^*e^{i\theta_+^*}) &= 0.140 \pm 0.093(\text{stat.}) \pm 0.028(\text{exp. syst.}) \pm 0.025(\text{model syst.}) \ , \\
y_+^* \equiv \Im(r_{B+}^*e^{i\theta_+^*}) &= 0.013 \pm 0.120(\text{stat.}) \pm 0.037(\text{exp. syst.}) \pm 0.056(\text{model syst.}) \ ,
\end{aligned}
$$

where $\theta_\pm^{(*)} = \delta^{(*)} \pm \gamma$, with γ the CKM weak phase, $\delta^{(*)}$ the strong phase of the $B^- \to D^{(*)0}K^-$ decay, and $r_B{}^{(*)}$ the absolute value of the ratio of the corresponding $A(b \to u)$ and $A(b \to c)$ amplitudes, $r_B = |A(b \to u)/A(b \to c)|$. The first errors are statistical, the second are experimental systematics and the third are due to the Dalitz model assumptions. The correlations of the pairs (x_-, y_-), (x_+, y_+), (x_-^*, y_-^*), and (x_+^*, y_+^*), are 3%, 6%, -17%, and -27%, respectively. All the other correlation terms are zero.

A classical (frequentist) analysis of the previous results yields the following results for the *CP*-violating parameters γ, $\delta^{(*)}$ and $r_B{}^{(*)}$:

$$
\begin{aligned}
\gamma &= 70(250)^\circ \pm 31^\circ(\text{stat.})^{+12^\circ}_{-10^\circ}(\text{exp. syst.})^{+14^\circ}_{-11^\circ}(\text{model syst.}) \quad [13^\circ, 136^\circ] \ , \\
\delta &= 104(284)^\circ \pm 45^\circ(\text{stat.})^{+17^\circ}_{-21^\circ}(\text{exp. syst.})^{+16^\circ}_{-24^\circ}(\text{model syst.}) \quad [0^\circ, 360^\circ] \ , \\
\delta^* &= 296(116)^\circ \pm 41^\circ(\text{stat.})^{+14^\circ}_{-12^\circ}(\text{exp. syst.}) \pm 15^\circ(\text{model syst.}) \quad [0^\circ, 360^\circ] \ , \\
r_B &= 0.118 \pm 0.079(\text{stat.}) \pm 0.034(\text{exp. syst.})^{+0.036}_{-0.034}(\text{model syst.}) \quad [0, 0.277] \ , \\
r_B^* &= 0.169 \pm 0.096(\text{stat.})^{+0.030}_{-0.028}(\text{exp. syst.})^{+0.029}_{-0.026}(\text{model syst.}) \quad [0, 0.352] \ .
\end{aligned}
$$

The first errors are statistical, the second are experimental systematics and the third are due to the Dalitz model. For γ and $\delta^{(*)}$ the $\pm 180^\circ$ ambiguity solutions are also given. The values inside square brackets indicate the 1.96 standard deviation intervals (95% confidence-level for a 1-dimensional Gaussian distribution). The significance of *CP* violation is 2.4 standard deviations. These results agree fairly well with those obtained using a Bayesian technique with flat prior for γ, $\delta^{(*)}$ and $r_B{}^{(*)}$.

A Cartesian coordinates: Toy MC studies

Extensive Toy MC studies have been performed in order to verify the Gaussian behavior of the errors of the cartesian fit variables.

Figures 30 and 31 show the residual, error and pull distributions of the cartesian fit parameters obtained from a set of about 2K Toy MC experiments corresponding to the nominal fit to the data sample. The arrows show the results found in the data. The goodness-of-fit, estimated by counting the number of experiments with a likelihood value larger than that found in the data, is around 50%, perfectly in agreement with the value found when the fit is performed in polar coordinates [2]. Similarly, figure 32 shows all the correlation coefficients for the two samples. From these figures we conclude that the cartesian fit parameters space behaves to an excellent approximation as single and independent Gaussians. The little (on average) correlation for the pair of variables (x_+, y_+) and (x_-, y_-) within a sample (D^0K or $D^{*0}K$) is taken into account in the PDF of the fitted parameters as a function of the generated parameters. The agreement between the simulation and the data is remarkable. From a closer look at the residual and pull distributions it is observed that in some case the mean values of the distributions are slightly biases. These biases are in all cases one order of magnitude below the statistical precision, and are due to the limited precision in the numerical Dalitz PDF normalization. Increasing the precision from the nominal 200×200 grid to 1000×1000 the biases essentially disappear.

Figures 33 and 34 show the residual distributions together with their mean values and rms of $(x_\pm, y_\pm)$ for D^0K and $D^{*0}K$, in 6 bins (0.05 units width each) of r_B truth. Despite the large (unrealistic) range of r_B truth, the width of the distributions are in all cases consistent within 10%, with no significant biases. Similarly, figures 35 and 36 show the corresponding pull distributions, which have widths always consistent with unity.

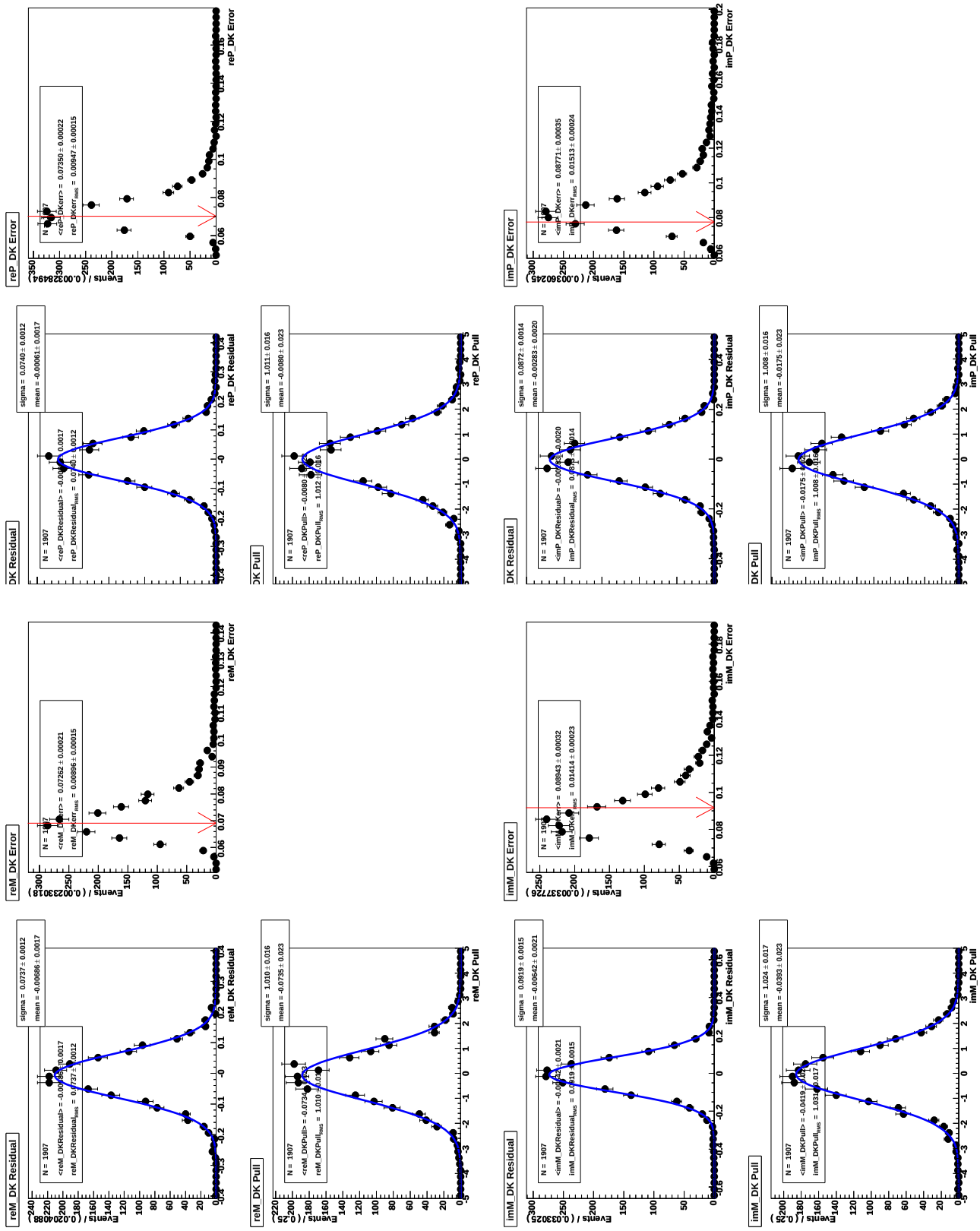

Figure 30: *Residual, error and pull distributions for x_+ (top left in landscape), y_+ (top right in landscape), x_- (bottom left in landscape) and y_- (bottom right in landscape) for the D^0K sample for the nominal Toy MC. The arrows show the results found in the data.*

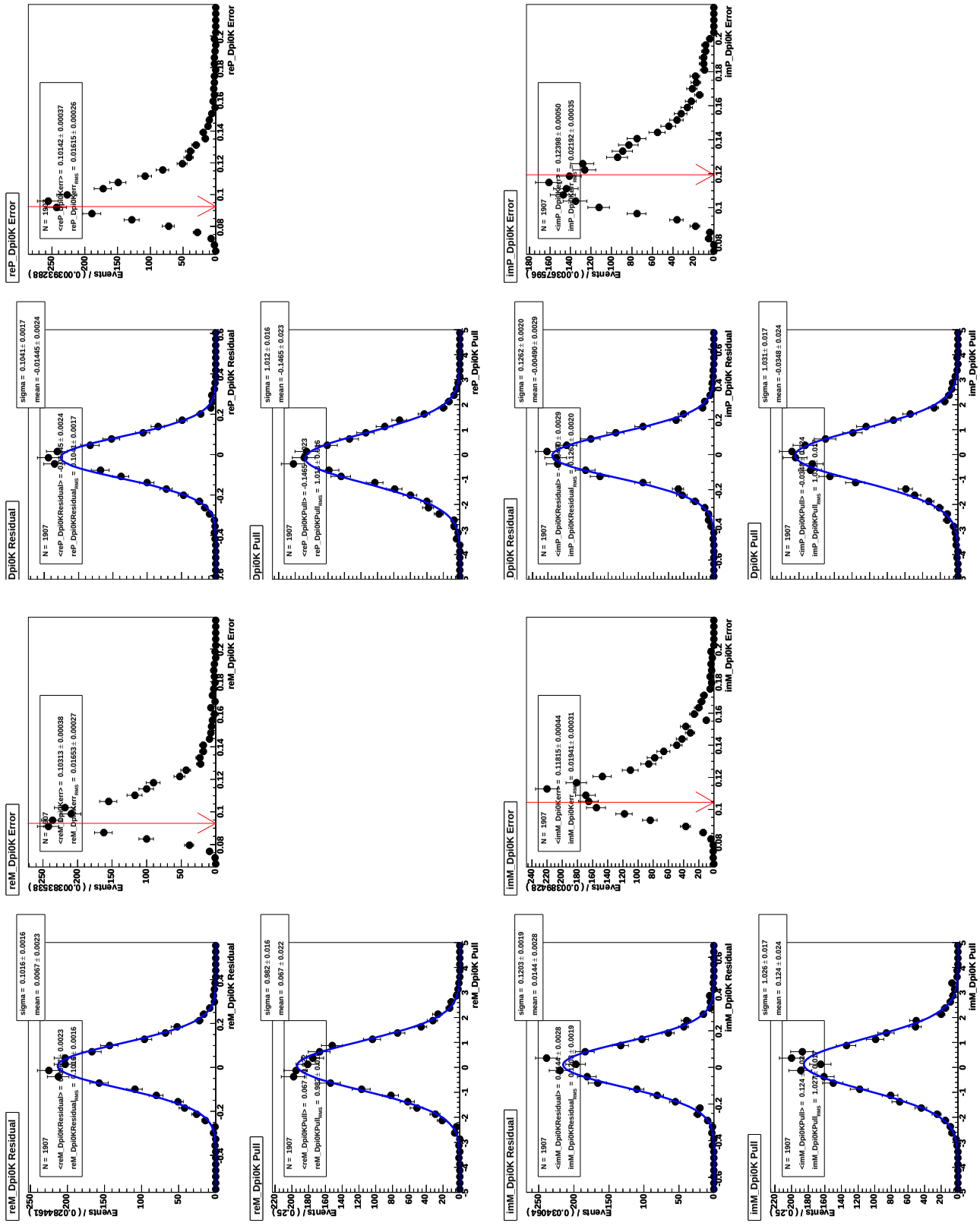

Figure 31: *Residual, error and pull distributions for x_+ (top left in landscape), y_+ (top right in landscape), x_- (bottom left in landscape) and y_- (bottom right in landscape) for the $D^{*0}K$ sample for the nominal Toy MC. The arrows show the results found in the data.*

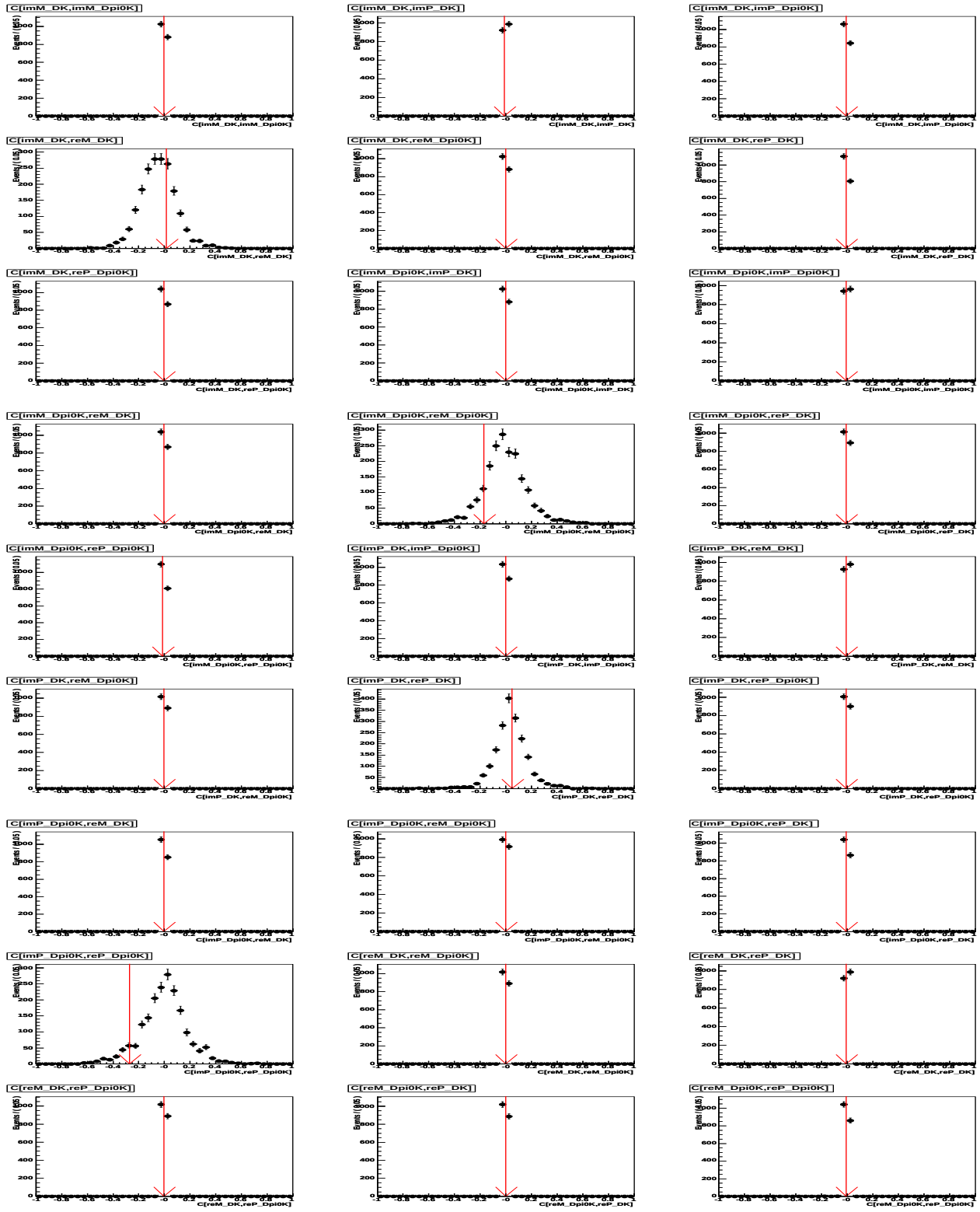

Figure 32: *Correlation coefficients among $(x_\pm, y_\pm)$ fit parameters for the D^0K and $D^{*0}K$ samples for the nominal Toy MC. The arrows show the results found in the data. It is clearly seen that the only non zero correlations appear for the pairs (x_+, y_+) and (x_-, y_-) within a given sample.*

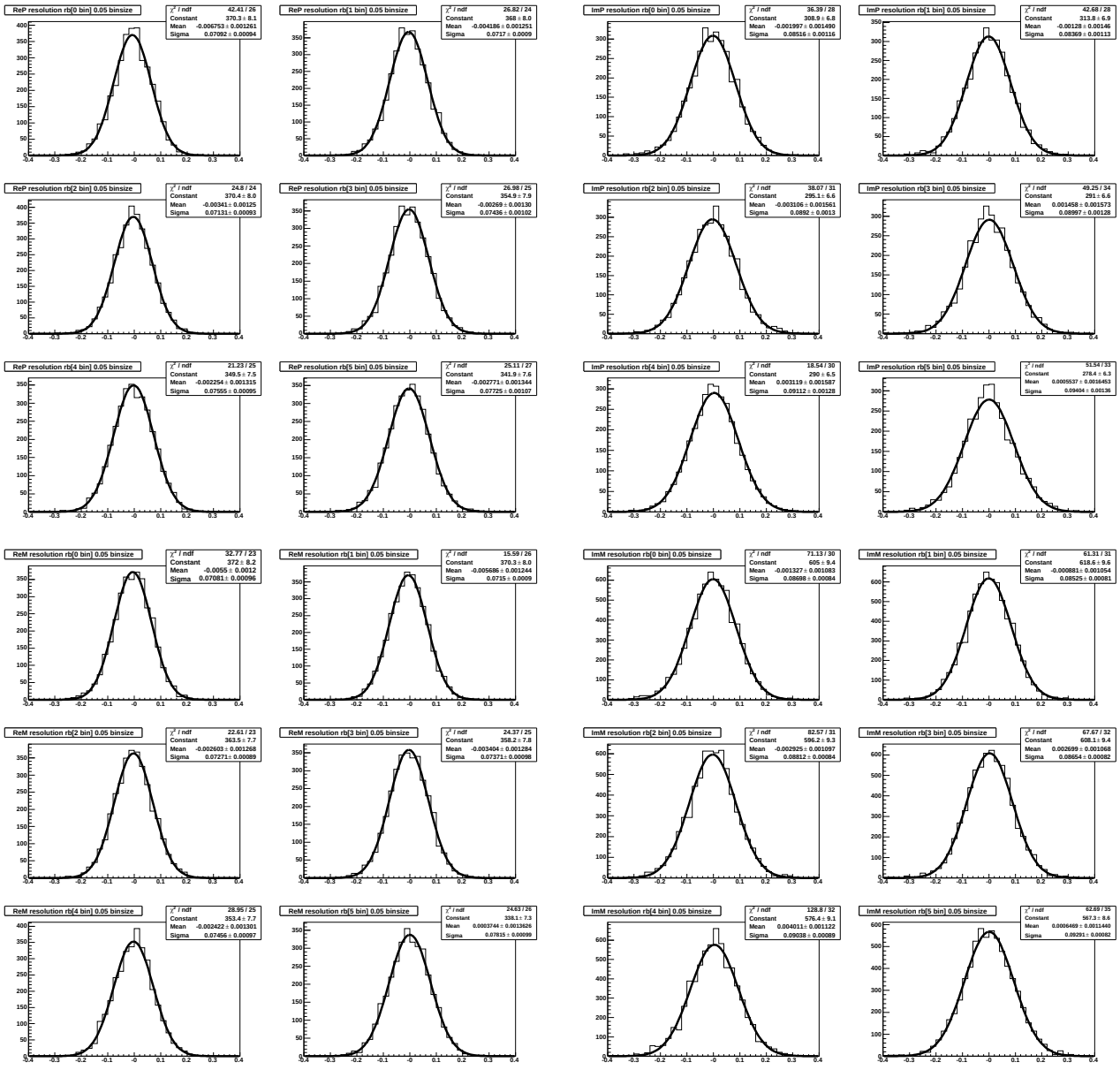

Figure 33: *Dependence of the rms of* $(x_\pm, y_\pm)$ *residual distributions,* $(\sigma_{x_\pm}, \sigma_{y_\pm})$*, in 6 bins of the truth* r_B *value, for the* D^0K *mode. The truth (generated) value of* r_B *has been obtained randomly in the range* $[0, 0.3]$*. As the the truth phases (both* γ *and* δ*) have also been generated randomly the obtained rms is averaged over all possible values of the phases.*

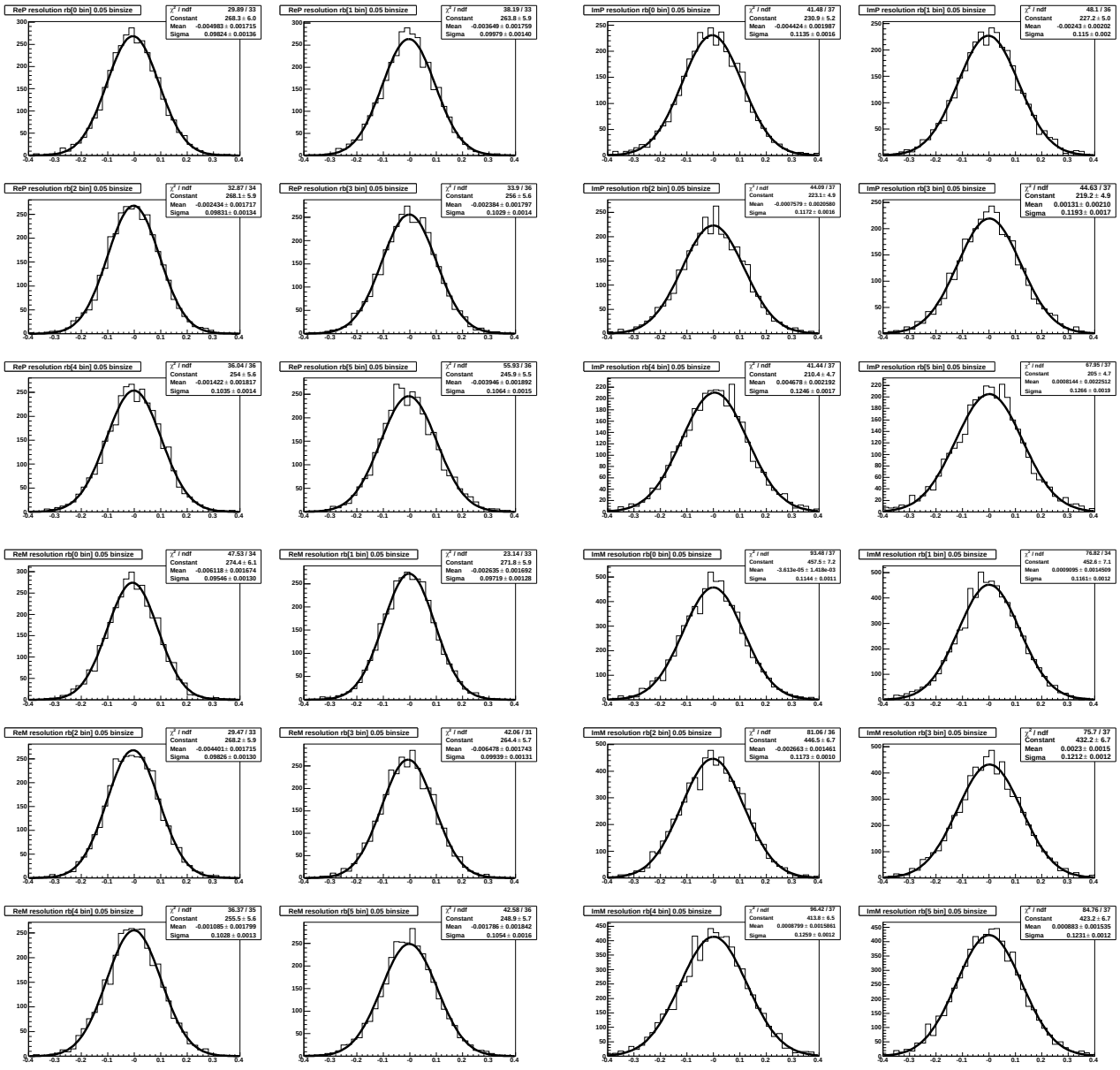

Figure 34: *Dependence of the rms of* $(x_\pm, y_\pm)$ *residual distributions,* $(\sigma_{x_\pm}, \sigma_{y_\pm})$*, in 6 bins of the truth* r_B *value, for the* $D^{*0}K$ *mode. The truth (generated) value of* r_B *has been obtained randomly in the range* $[0, 0.3]$*. As the the truth phases (both* γ *and* δ*) have also been generated randomly the obtained rms is averaged over all possible values of the phases.*

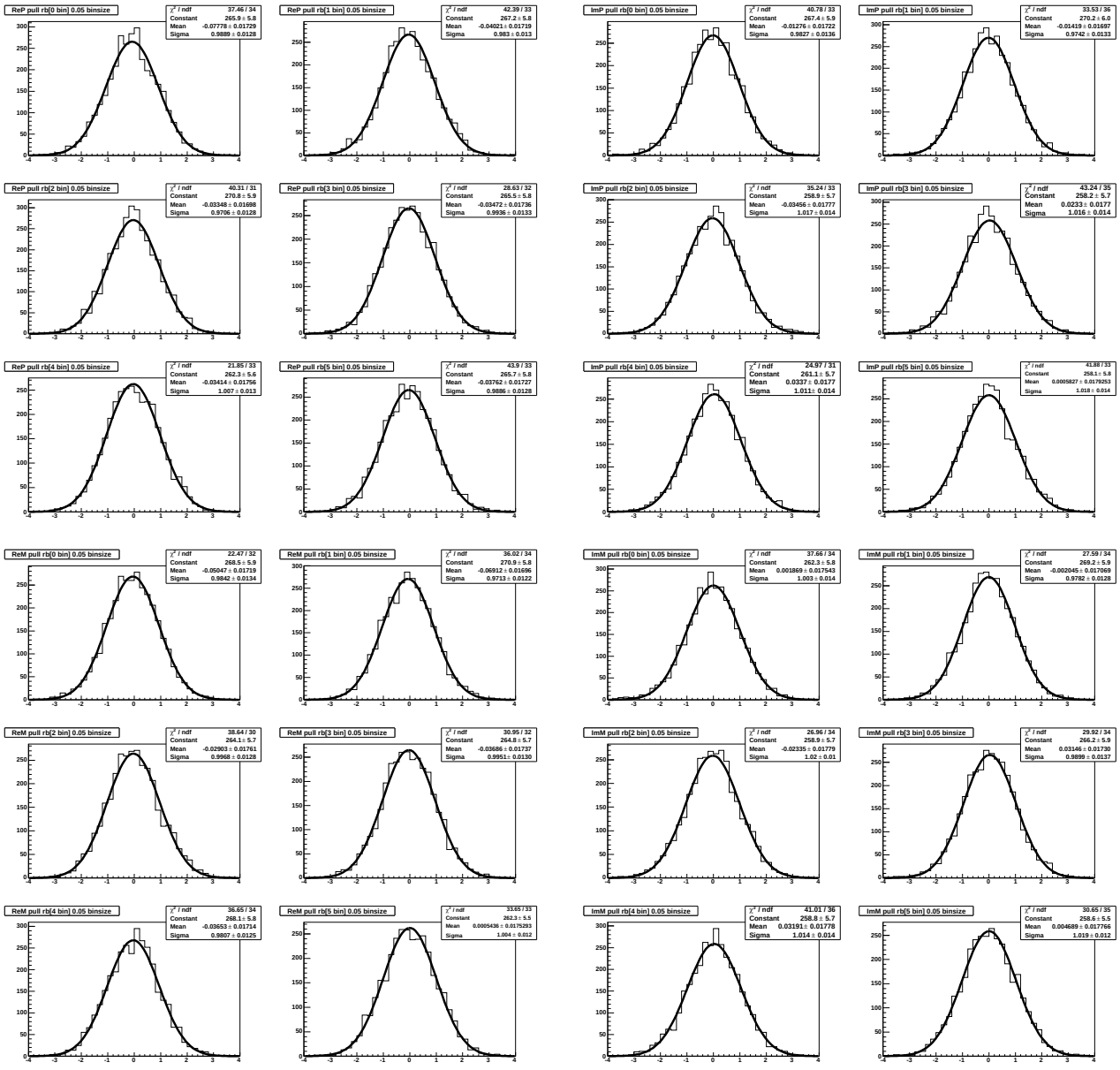

Figure 35: *Dependence of the rms of* $(x_{\pm}, y_{\pm})$ *pull (residual normalized to the error) distributions in 6 bins of the truth* r_B *value, for the* D^0K *mode. The truth (generated) value of* r_B *has been obtained randomly in the range* $[0, 0.3]$*. As the the truth phases (both* γ *and* δ*) have also been generated randomly the obtained rms is averaged over all possible values of the phases.*

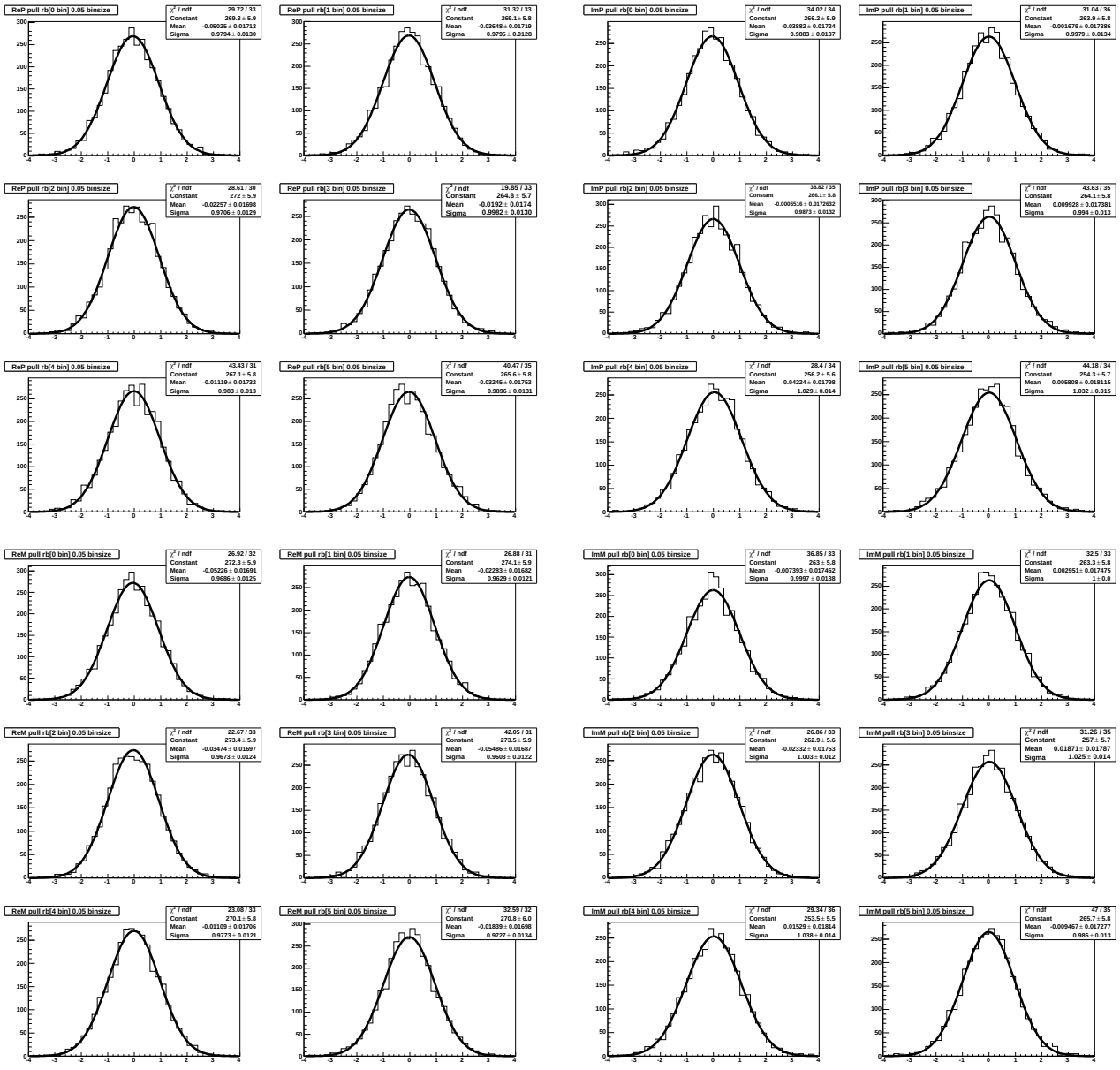

Figure 36: *Dependence of the rms of* $(x_{\pm}, y_{\pm})$ *pull (residual normalized to the error) distributions in 6 bins of the truth* r_B *value, for the* $D^{*0}K$ *mode. The truth (generated) value of* r_B *has been obtained randomly in the range* $[0, 0.3]$*. As the the truth phases (both* γ *and* δ*) have also been generated randomly the obtained rms is averaged over all possible values of the phases.*

B Confidence regions for D^0K null data point

As a control check of the method, we have tested the whole frequentist procedure with a null measured point (i.e. $r_B = 0$, or equivalently $\mathbf{z}_\pm = 0$). For this check we have taken for $(\sigma_{x_\pm}, \sigma_{y_\pm})$ and $\rho_\pm$ the values of the D^0K sample. The 2- and 1-dimensional projections of the 3-dimensional regions for this null test are shown in figures 37 and 38. It can be seen that the 19.9% region (68.3% for 1-dimensional projections) perfectly covers $r_B = 0$, and there is no information at all about the phases, as expected.

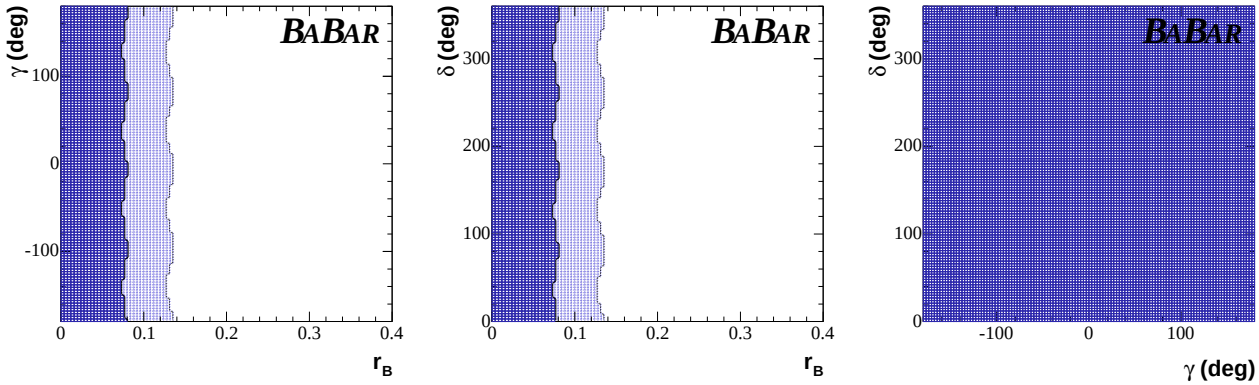

Figure 37: *2-dimensional projections of the 19.9% (red/dark) and 72.1% (yellow/light) confidence-level 3-dimensional regions for the null hypothesis using the D^0K mode.*

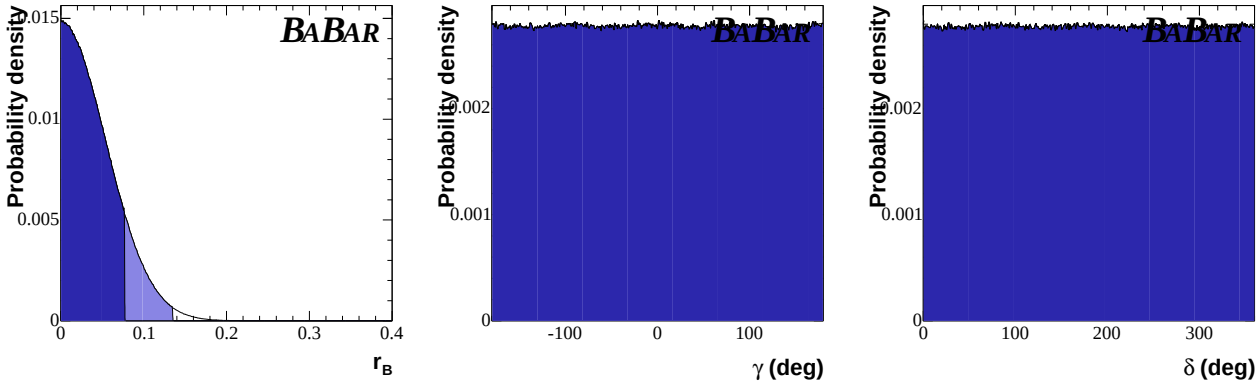

Figure 38: *Probability density functions for r_B, γ and δ together with the 1-dimensional projections of the 19.9% (red/dark) and 72.1% (yellow/light) confidence-level 3-dimensional regions for the null hyphotesis in the D^0K mode.*

C Confidence regions for $D^0\pi$ null data point

As an additional control check of the *CP* violation sensitivity of the $D^0\pi$ and $D^{*0}\pi$ samples, we have repeated the frequentist procedure with a null measured point (i.e. $r_B = 0$, or equivalently $\mathbf{z}_\pm = 0$) with $(\sigma_{x_\pm}, \sigma_{y_\pm})$ and $\rho_\pm$ values identical to those of the $D^0\pi$ sample. The 2- and 1-dimensional projections of the 3-dimensional regions for this $D^0\pi$ null test are shown in figures 39 and 40. It can be seen that the 19.9% region (68.3% for 1-dimensional projections) perfectly covers $r_B = 0$, and there is no information at all about the phases, as expected.

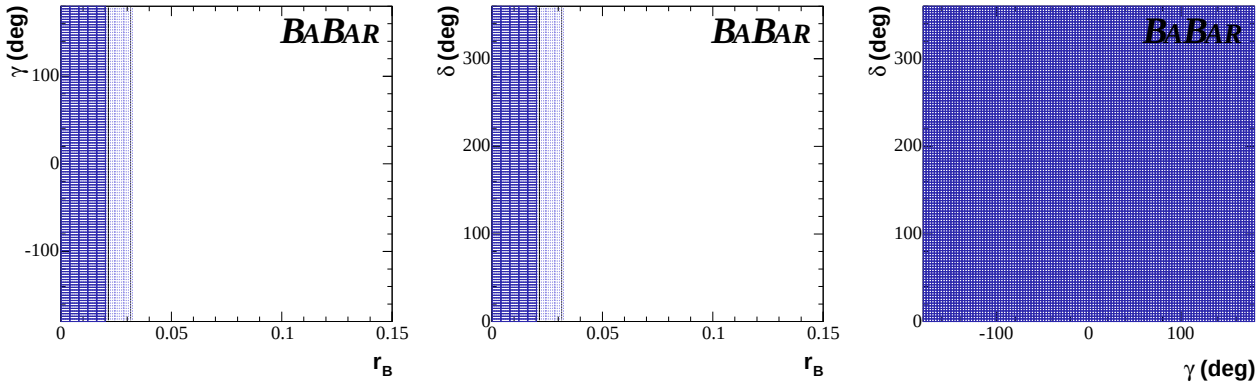

Figure 39: *2-dimensional projections of the 19.9% (red/dark) and 72.1% (yellow/light) confidence-level 3-dimensional regions for the null hypothesis using the $D^0\pi$ mode.*

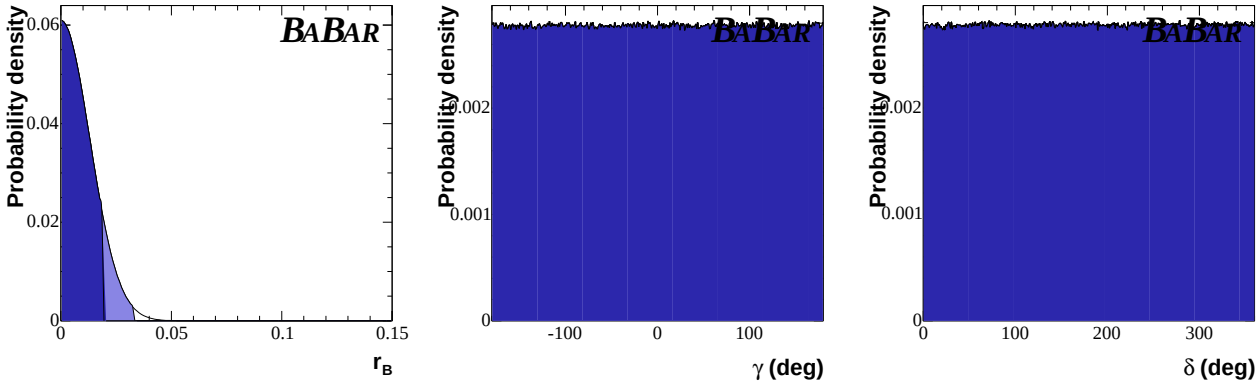

Figure 40: *Probability density functions for r_B, γ and δ together with the 1-dimensional projections of the 19.9% (red/dark) and 72.1% (yellow/light) confidence-level 3-dimensional regions for the null hyphotesis in the $D^0\pi$ mode.*

References

[1] A. Giri, Yu. Grossman, A. Soffer and J. Zupan, *Phys. Rev.* **D68**, 054018 (2003).

[2] Extraction of the CKM angle γ in $B^- \to D^{(*)}K^-$ decays using a D^0 Dalitz plot analysis, *BABAR* Analysis Document #899.

[3] S. Eidelman *et al.* [Particle Data Group Collaboration], Phys. Lett. B **592**, 1 (2004) (section on Statistics). See also for example: G. Zech, (hep-ex/0106023).

[4] A. Poluektov et al (Belle Coll.), Phys. Rev. D **70** 072003 (2004).

[5] G.J. Feldman and R.D. Cousins, Phys. Rev. D **57** 3873 (1998).

[6] A. Palano, Dalitz plot analysis of $D^0 \to K^0_S\pi^+\pi^-$, $D^0 \to K^0_S K^+\pi^-$, and $D^0 \to K^0_S K^+K^-$, **BAD 120**.

[7] K. M. Watson, Phys. Rev. **88** 1163 (1952).